



Applicability assessment of functional adsorption zeolite materials in adsorption desalination cum cooling systems driven by low-grade heat source

Seong-Yong Woo^{a,1}, Ho-Saeng Lee^{b,1}, Jun-Sik Kim^a, Kyung-Hun Kim^a, Ho Ji^b, Young-Deuk Kim^{c,d,*}

^a Department of Mechanical Design Engineering, Hanyang University, 222 Wangsimni-ro, Seongdong-gu, Seoul 04763, Republic of Korea

^b Seawater Utilization Plant Research Center (SUPRC), Korea Research Institute of Ships & Ocean Engineering, 124-32 Simcheungsu-gil, Jukwang-myeon, Goseong-gun, Gangwon-do 219-822, Republic of Korea

^c Department of Mechanical Engineering, Hanyang University, 55 Hanyangdaehak-ro, Sangnok-gu, Ansan, Gyeonggi-do 15588, Republic of Korea

^d BK21 FOUR ERICA-ACE Center, Hanyang University, 55 Hanyangdaehak-ro, Sangnok-gu, Ansan, Gyeonggi-do 15588, Republic of Korea

ARTICLE INFO

Keywords:

Adsorption desalination
Functional adsorbent material
Adsorption isotherm
Performance evaluation

ABSTRACT

This study provides an in-depth analysis of the sequence of procedures required to evaluate the performance of adsorption desalination (AD) using functional adsorbent material zeolites (i.e., FAM-Z series with AFI and CHA types). The applicability of zeolite as an adsorbent for the AD cycle was also demonstrated by comparing it with the performance of AD using silica gel. The adsorption isotherm of the adsorbent, which is the most important parameter in the performance and design of the AD cycle, is recognized as a crucial parameter that significantly affects the AD performance. The thermophysical properties of the FAM-Z series were analyzed using argon adsorption and desorption isotherms at 87 K, followed by water vapor adsorption isotherms. Modified Do-Do and hybrid Langmuir-Sips isotherm models were proposed and are suitable for the anomalous stepwise isotherms of the FAM-Z series and the mesoporous adsorption characteristics of silica gel. The performance of the AD cycle was assessed in terms of the specific daily water production, specific cooling capacity, coefficient of performance, and performance ratio with respect to chilled and hot water temperatures and cycle times using a mathematical model of the AD cycle validated through a comparison with experimental data. AFI-type zeolites showed the applicability of residential (FAM-Z01) and district cooling (FAM-Z05), which have a low regeneration temperature of 55 °C owing to an unusual isotherm (i.e., sigmoid adsorption isotherm). In addition, FAM-Z05 exhibited considerable potential as an adsorbent for AD cycles driven by extremely low-grade heat sources (<55 °C) found in industrial plants and solar energy.

1. Introduction

Water scarcity and global warming have intensified owing to industrial development and population growth; hence, it is essential to develop promising technologies to meet the growing demand for desalinated water and energy. The largest amount of available but unused low-temperature heat is usually found in industrial plants and solar energy, and many studies have been conducted on environmentally friendly and high-efficiency systems driven by low-grade heat sources. Among them, adsorption systems that exploit the physical and

thermodynamic characteristics of adsorbents and adsorbates (e.g., chillers, heat pumps, and desalination plants) have the following advantages: (i) They work effectively at relatively low heat source temperatures (50 °C to 80 °C), such as waste heat and solar energy, reducing the operating costs and CO₂ emissions. (ii) It has no major moving parts, incurring low maintenance costs. (iii) It utilizes no chemicals in the pretreatment process. Finally, (iv) it operates at low pressures and temperatures, minimizing fouling and scaling [1,2].

Adsorption desalination (AD) has received a great deal of attention because it produces two useful effects, i.e., high-grade freshwater and a cooling capacity, with a nearly consistent performance regardless of

* Corresponding author at: Department of Mechanical Engineering, Hanyang University, 55 Hanyangdaehak-ro, Sangnok-gu, Ansan, Gyeonggi-do 15588, Republic of Korea.

E-mail address: youngdeuk@hanyang.ac.kr (Y.-D. Kim).

¹ These authors contributed equally to this article.

<https://doi.org/10.1016/j.cej.2021.131375>

Received 20 April 2021; Received in revised form 29 June 2021; Accepted 15 July 2021

Available online 21 July 2021

1385-8947/© 2021 Elsevier B.V. All rights reserved.

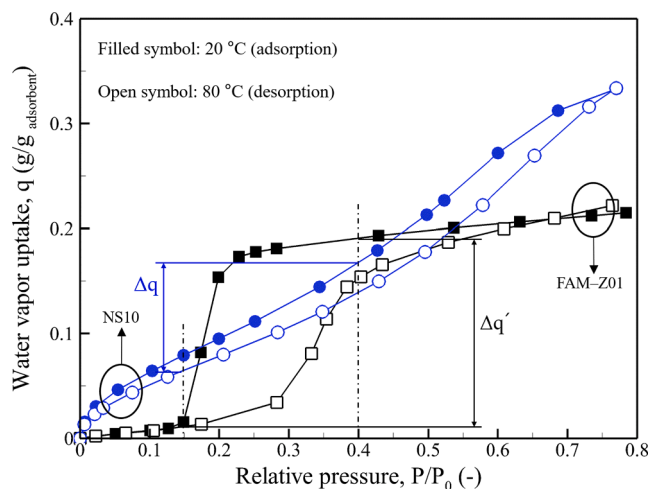


Fig. 1. Schematic of equilibrium adsorption isotherms (FAM-Z01 and NS10) illustrating the effect of net equilibrium adsorption capacity (Δq) on the performance of adsorption desalination and cooling system. The filled and open symbols denote the adsorption isotherms at low (i.e., adsorption) and high (i.e., desorption) temperatures, respectively. In addition, P/P_0 along the transverse axis is the relative pressure ratio, defined as the ratio of the water vapor pressure to the saturation vapor pressure at the adsorbent temperature. Finally, q along the vertical axis is the specific equilibrium water uptake.

Table 1
Summary of previous studies on adsorption systems using the FAM-Z series.

| Adsorbent | Application | Description | Performance |
|---------------------------------------|--------------|---|---|
| FAM-Z01 FAM-Z02 FAM-Z05 [17] | chiller | numerical simulation 2-bed conventional adsorption chiller system | SCP: 51 RT/tonne (FAM-Z01), 72 RT/tonne (FAM-Z02), and 7.5 RT/tonne (FAM-Z05) at hot-water temperature of 80 °C COP: 0.48 (FAM-Z01), 0.42 (FAM-Z02), and 0.18 (FAM-Z05) at hot-water temperature of 80 °C |
| FAM-Z01 [19] | chiller | numerical simulation 2-bed adsorption chiller system | COP: 0.44 (hot-water temperature of 65 °C at half-cycle time of 400 s) |
| FAM-Z02 [20] | desalination | numerical simulation 4-bed adsorption desalination system | SDWP: 6.3 m ³ /tonne-day (hot-water temperature of 85 °C at half-cycle time of 300 s) SCP: 53.7 RT/tonne |
| FAM-Z02 [21] | desalination | numerical simulation 4-bed adsorption desalination system | SDWP: 4.9 m ³ /tonne-day (single stage), 6.64 m ³ /tonne-day (2-stage), and 12.4 m ³ /tonne-day (2-stage with heat recovery) at hot-water temperature of 85 °C SCP: 43 RT/tonne (single stage), 46.6 RT/tonne (2-stage), and 32.4 RT/tonne (2-stage with heat recovery) |
| FAM-Z02 [22] | chiller | experimental investigation compact chiller for automobiles 2-bed adsorption chiller system | SCP: 117 RT/tonne (hot-water temperature of 80 °C) COP: 0.31 |
| FAM-Z01 FAM-Z05 [23] | chiller | numerical simulation use of FAM-Z01 (in low pressure bed) and -Z05 (in high pressure bed) 3-bed adsorption chiller system | COP: 0.36 (hot-water temperature of 52 °C and chilled water temperature of 10 °C) |

of the FAM-Z series for predicting the performance of adsorption systems. In addition, few studies have evaluated AD performance with respect to key operating parameters (i.e., hot and chilled water temperatures and cycle times) using all FAM-Z series (i.e., FAM-Z01, -Z02, and -Z05).

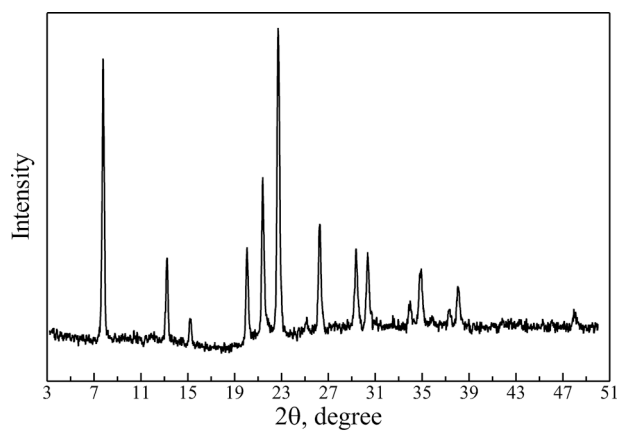
This study presents detailed experimental and theoretical approaches for evaluating the performance of the AD cycle. The applicability of zeolites (i.e., FAM-Z series with AFI and CHA types) as an adsorbent for the AD cycle was demonstrated through a comparison with the performance of AD using silica gel (i.e., NS10). The potential for applying an extremely low-grade (<55 °C) waste heat commonly found in industrial plants and solar energy was also evaluated. First, the physical properties of the zeolites were rigorously analyzed using the adsorption and desorption isotherms of argon at 87 K, eliminating the possibility of interaction with surface functional groups or exposed ions. This was followed by an evaluation of water vapor adsorption isotherms over a wide relative pressure range ($0 < P/P_0 < 0.8$) at temperatures of between 20 °C and 80 °C, and the adsorption characteristics of the FAM-Z series were thoroughly investigated. To satisfactorily fit the unusual adsorption isotherm (i.e., low adsorption at low pressure followed by a rapid water vapor uptake for FAM-Z01 and FAM-Z05, and high adsorption at low pressure followed by asymptotic water vapor uptake for FAM-Z02) and adsorption isotherm of NS10 with mesoporous characteristics, modified Do-Do and hybrid Langmuir-Sips isotherm models are proposed. Here, the isotherm model considering the thermophysical parameter (i.e., isosteric enthalpy) estimated by Clausius-Clapeyron and Henry's equations was evaluated by comparing the adsorption isotherms of the adsorbent. The coefficient of determination (R^2) was used to assess the degree of fit between the measured isotherm data and adsorption isotherm model. The AD performance was evaluated with respect to key parameters (i.e., hot and chilled water temperatures and cycle times) in terms of the specific daily water production (SDWP), specific cooling capacity (SCC), coefficient of performance (COP), and performance ratio (PR) using a mathematical model of the AD cycle validated through a comparison with the experimental data.

2. Experimental section

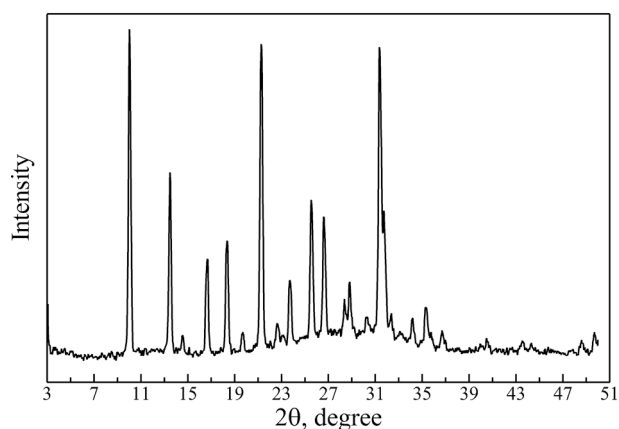
2.1. Materials

The structure and crystallinities of the FAM-Z series were determined through X-ray diffraction (XRD) (D8 Advance, Bruker, USA) using Ni-filtered Cu-K α radiation ($\lambda = 1.5418 \text{ \AA}$) and a step size of 0.02° over the range of $3^\circ < 2\theta < 50^\circ$. According to the XRD pattern (Fig. 2a and 2c), FAM-Z01 and Z05 showed typical features of the AFI structure and had a one-dimensional structure [15]. Meanwhile, FAM-Z02 displayed a CHA type having a three-dimensional structure with large ellipsoidal cages where characteristic diffraction peaks appear at $2\theta = 8^\circ, 16^\circ, 21^\circ, 26^\circ,$ and 32° (Fig. 2b). Most of the XRD peaks were sharp, indicating that the FAM-Z series achieved good crystallinity [14].

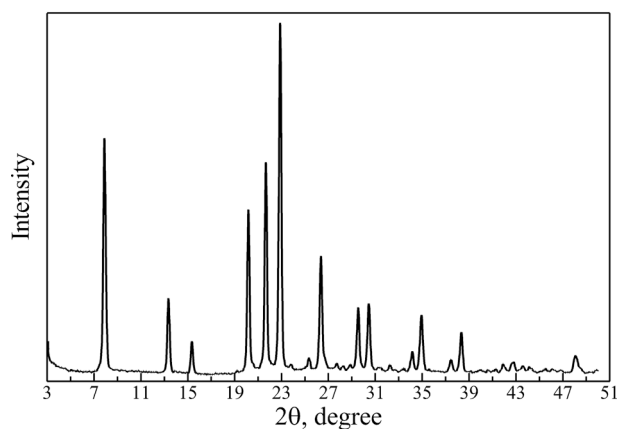
Morphological and structural analyses were conducted using scanning electron microscopy, and the SEM images of the adsorbents are as shown in Fig. 3. AFI-type zeolites such as FAM-Z01 and FAM-Z05 are ferroaluminophosphate (FAPO-5) and aluminophosphate-(AlPO-5) based zeolites [12]. FAM-Z01 consists of AlO_4 , PO_4 , and FeO_4 tetrahedra, where Al and P atoms are partially replaced by Fe atoms, whereas FAM-Z05 is only fabricated using AlO_4 and PO_4 [16]. The CHA-type zeolite (i.e., FAM-Z02) is a silico-aluminophosphate (SAPO-34) zeotype and is composed of AlO_4 , PO_4 , and SiO_4 , where Al and P atoms are partially substituted by Si atoms [17]. It was clearly observed that AFI-type zeolites have an elongated plate structure, whereas CHA-type zeolites have a regular cubic or brick structure. Meanwhile, a partial destruction of the plate structure was observed (Fig. 3a) for FAM-Z01 owing to its brittleness [14]. NS10 consisted of 15 wt% Al_2O_3 and 85 wt% SiO_2 . This enabled repeated adsorption and desorption of vapor through improvements in the mechanical strength of the silica-based adsorbent [3], and Al_2O_3 impregnated on the



(a)



(b)



(c)

Fig. 2. XRD pattern of FAM-Z series: (a) FAM-Z01, (b) FAM-Z02, and (c) FAM-Z05.

surface of NS10 was observed (Fig. 3d).

2.2. Experimental equipment

2.2.1. Adsorption analyzers

To investigate the physical properties of NS10, its adsorption and

desorption isotherms were examined using an analyzer (3Flex, Micromeritics Instrument Co., USA) with a static volumetric method at 77 K of nitrogen; here, NS10 was outgassed at 393.15 K for 6 h under a vacuum of 10^{-4} Pa prior to the adsorption measurements. Although nitrogen is generally accepted as a standard adsorbate for analyzing the physical properties of an adsorbent, it yields unsatisfactory results for microporous or polar materials such as zeolites, metal oxides, and MOFs. This is because the quadrupole moment of nitrogen can interact with various surface functional groups and exposed ions within the adsorbents, resulting in uncertainty of the cross-sectional area used for BET surface area calculations [25]. By contrast, monoatomic argon has no dipole or quadrupole moments, which allows for a consistent orientation on the surface of the adsorbent and a clear cross-sectional area. Therefore, the International Union of Pure and Applied Chemistry (IUPAC) recommended the use of argon to assess the physical properties of microporous or polar materials [26,27]. In this study, the adsorption and desorption isotherms of the zeolites were investigated using an analyzer (Autosorb iQMP, Quantachrome Instrument, USA) at 87 K of argon.

To evaluate the applicability of the adsorbents in the AD cycle using low-temperature heat sources, their water vapor uptake characteristics were examined using a volumetric adsorption analyzer (VSTAR2, Anton Paar QuantaTec Inc., USA). Here, the water vapor uptake was investigated over a wide relative pressure range ($0 < P/P_0 < 0.8$) at temperatures of between 20 °C and 80 °C. Here, the FAM-Z series was outgassed at 433.15 K for 6 h under a vacuum of 10^{-4} Pa prior to the measurements of adsorption of argon and water vapor.

2.2.2. Pilot-scale AD system

As shown in Fig. 4, the AD system consists mainly of an evaporator (component 19), a condenser (component 7), and two beds (i.e., adsorber: component 2 and desorber: component 1), each containing fin-tube heat exchangers (component 4) filled with adsorbents (component 3). The pre-treated (e.g., filtering and deaeration) seawater in the deaeration tank (component 16) is fed into the evaporator, and high-grade distillate is extracted from the condenser. Here, the seawater is fed into the evaporator depending on the amount and level of seawater required to sustain a continuous evaporation, and the brine is discharged when the concentration reaches a predetermined limit. The evaporation of seawater is initiated by the affinity of the adsorbent for water vapor and vapor introduced into the adsorber through the vapor line (component 5), which is attributed to the driving force (e.g., van der Waals force and weak electrostatic force). The vapor is adsorbed on the surface of the adsorbent through physical adsorption, and the chilled water (component 21) produced by the latent heat of the vaporization can be used for the air-conditioning process. The adsorption heat is released during the phase change from gas to liquid (i.e., the exothermic reaction during physisorption) and removed by the cooling water circulating in the tube of the fin-tube heat exchanger in the adsorber. This adsorption process was continued over a half-cycle and then switched to the preheating mode for transition to the desorption process. During the preheating mode, a low-temperature (50 °C to 80 °C) heat source (i.e., hot water) is supplied to the fin-tube heat exchanger of the adsorber, which is isolated by closing the vapor lines (components 5 and 6), thereby increasing the vapor pressure in the adsorber. The kinetic energy of the water vapor adsorbed in the adsorbent is increased to attain the threshold kinetic energy, and water vapor can desorb from the adsorbent; this is called the desorption process.

The desorbed water vapor traveled from the desorber to the condenser through the vapor line (component 6), and the latent heat was removed by circulating the cooling water. The desorbed water vapor is condensed on the outer surface of the tube bundle in the condenser, and high-grade condensate was continuously collected in the freshwater collection tank by gravity (component 15). This desorption process was continued over a half-cycle until it was switched to the pre-cooling mode for transition to the adsorption process. Another bed (component 1) is operated following a process that is the reverse of that mentioned above.

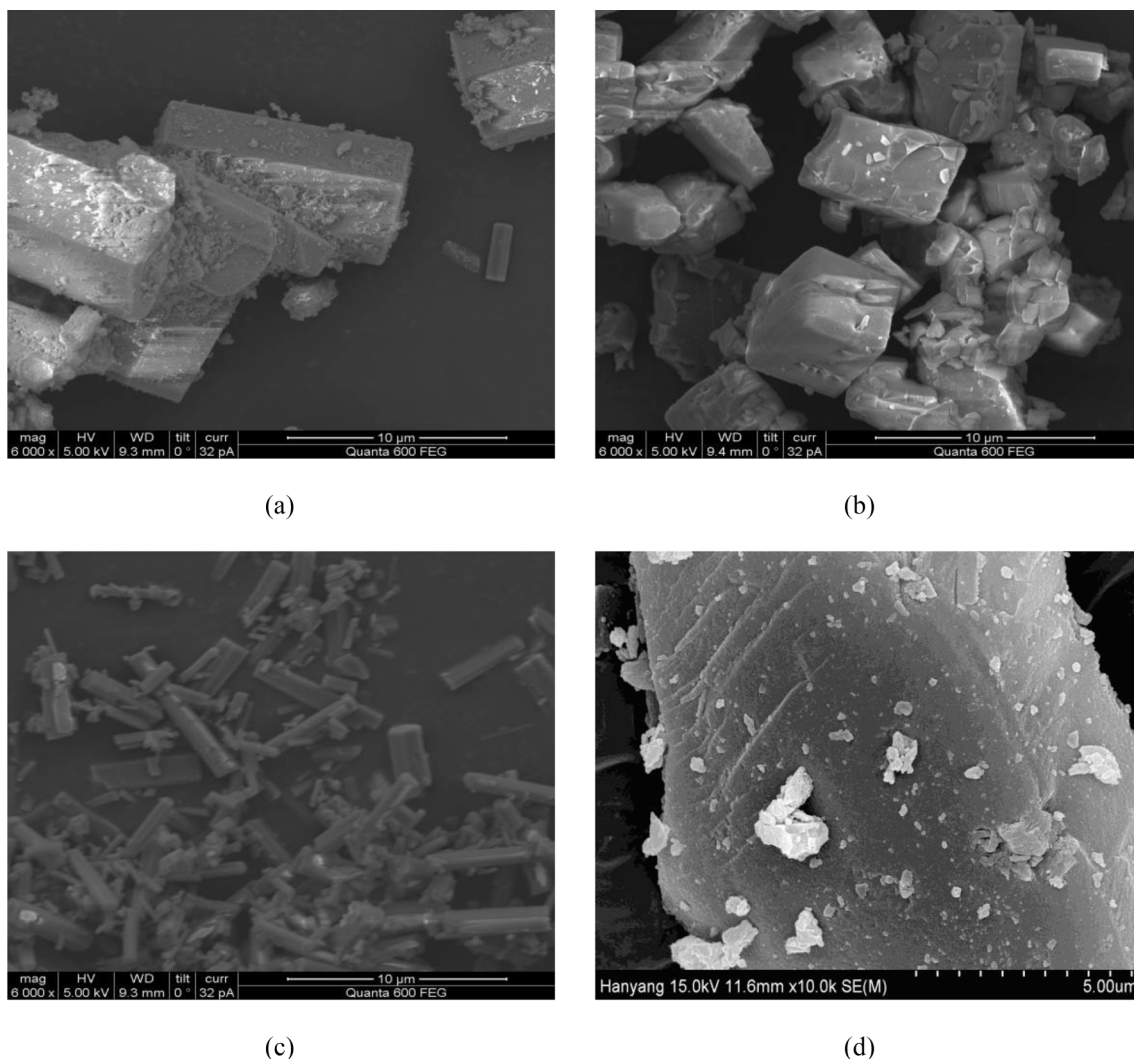


Fig. 3. SEM pictures of the adsorbents: (a) FAM-Z01, (b) FAM-Z02, (c) FAM-Z05, and (d) NS10.

Thus, the AD system was batch-operated concomitantly with adsorption-triggered-evaporation and desorption-activated-condensation processes. Fig. 5 shows a pilot-scale two-bed AD system using NS10 housed at Hanyang University (Republic of Korea).

3. Theoretical section

3.1. Adsorption isotherm models

Because the adsorption isotherm plays a key role in modeling the adsorption system and predicting its performance, it is essential to use an adsorption isotherm model that can more accurately predict the measured adsorption isotherm of the adsorbent applied to the system. In this study, modified Do–Do (AFI-type zeolites) and hybrid Langmuir–Sips isotherm models (CHA-type zeolite and silica gel) were proposed to replicate the equilibrium adsorption isotherms of water vapor on the adsorbents.

Do and Do proposed a model describing water vapor adsorption by activated carbon, which is an extremely microporous adsorbent, and the model is based on the assumption that adsorption proceeds through a two-stage mechanism. First, water molecules are strongly bonded to the primary adsorption sites and form a conglomerate of molecules through hydrogen bonds [28]. If the number of molecules is equal to six, the cluster of five molecules can tear away from the conglomerate and fill the micropores, resulting in a steep increase in water vapor uptake.

However, the size of the clusters is dependent on the pore width and distribution of the primary sites, indicating that the cluster size is not constant. Thus, Neitsch et al. proposed a modified Do–Do isotherm model to generalize the model in such a way that the size of the water clusters is variable [28]. The model can be expressed as follows:

$$q = q_s \frac{K_s \sum_{n=1}^N n(P/P_0)^n}{1 + K_s \sum_{n=1}^N (P/P_0)^n} + q_m \frac{K_m (P/P_0)^M}{1 + K_m (P/P_0)^M} \quad (1)$$

$$q_s = q_1 \exp\left(\frac{-\alpha}{RT}\right) \quad (2)$$

$$K_s = K_{0s} \exp\left(\frac{-\Delta H_s}{RT}\right) \quad (3)$$

$$q_m = q_2 \exp\left(\frac{-\beta}{RT}\right) \quad (4)$$

$$K_m = K_{0m} \exp\left(\frac{-\Delta H_m}{RT}\right) \quad (5)$$

where q_s is the water vapor uptake of surface active groups, R is the universal gas constant, K_s is the equilibrium constant for chemisorption and hydrogen bonding at the primary sites, K_0 is the pre-exponential factor, N ($N \geq M + 1$) is the maximum number of water molecules adsorbed on the surface sites, P is the partial pressure, P_0 is the

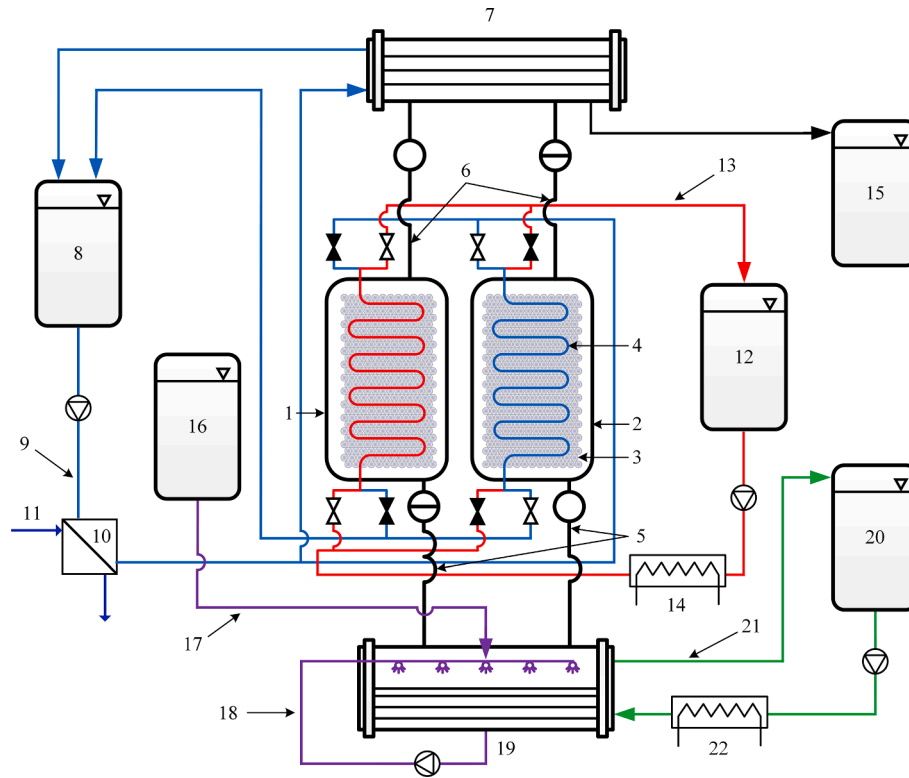


Fig. 4. Schematic of two-bed AD system (1, desorber; 2, adsorber; 3, adsorbent; 4, fin-tube heat exchanger; 5, 6, vapor line; 7, condenser; 8, cooling water tank; 9, cooling water line; 10, heat exchanger; 11, cooling water from cooling tower; 12, hot-water tank; 13, hot-water line; 14, electric heater; 15, freshwater collection tank; 16, deaeration tank; 17, seawater supply line; 18, brine circulation line; 19, evaporator; 20, chilled water tank; 21, chilled water line; 22, electric heater).

saturation pressure corresponding to the temperature of the adsorbent, q_m is the water vapor uptake by micropores, K_m is the micropore equilibrium constant, and ΔH_s and ΔH_m are isosteric enthalpies for chemical reaction and micropore filling, respectively. Here, the isosteric enthalpy of the adsorption can be estimated from the adsorption isotherm of water vapor using Clausius–Clapeyron (ΔH_s) and Henry's (ΔH_m) equations, respectively [12,16]. The Clausius–Clapeyron equation is written as follows:

$$\frac{\Delta H}{RT} = - \left[\frac{\partial \ln P}{\partial T} \right]_q \quad (6)$$

In addition, the isosteric enthalpy of the adsorption is given as

$$\ln P = \left(\frac{\Delta H}{R} \right) \frac{1}{T} + C \quad (7)$$

Meanwhile, a linear behavior is observed in Henry's region (i.e., $P/P_0 \approx 0$), and Henry's isotherm equation can be used to estimate the isosteric enthalpy at zero coverage (ΔH_m) [12].

$$q = K_H P \quad (8)$$

$$\ln K_H = - \left(\frac{\Delta H}{R} \right) \frac{1}{T} \quad (9)$$

where K_H is Henry's coefficient.

The Langmuir isotherm is the simplest isotherm model that is valid for describing micropore filling and monolayer adsorption, the major assumptions of which are as follows: (i) Molecules are adsorbed on a fixed number of well-defined localized sites, (ii) the adsorption energies of all adsorption sites are the same, (iii) there should be no steric hindrance or lateral interaction between the adsorbed molecules, (iv) adsorption occurs on a homogeneous surface where the sorption activation energy and enthalpy are constant through monolayer adsorption, (v) all sites should have equal affinity toward the adsorbate, and (vi) the

adsorption system is in dynamic equilibrium and the adsorption rate is the same as the desorption rate [29,30]. The Sips isotherm is a combination of the Langmuir and Freundlich isotherms, and is suitable for heterogeneous adsorption, capillary condensation, and saturation adsorption (i.e., limited adsorption capacity) [30,31]. Therefore, the proposed hybrid isotherm model can reproduce equilibrium adsorption isotherms with Langmuir isotherms at low pressure (i.e., micropore filling and monolayer adsorption) and Sips isotherms at moderate and high pressures (i.e., capillary condensation and saturation adsorption). The Langmuir–Sips hybrid isotherm can be expressed as follows:

$$q = q_{LS} \left(\frac{K_L(P/P_0)}{1 + K_L(P/P_0)} + \frac{K_S(P/P_0)^\theta}{1 + K_S(P/P_0)^\theta} \right) \quad (10)$$

$$q_{LS} = q_{max} \exp\left(\frac{-\alpha}{RT}\right) \quad (11)$$

$$K_L = K_{0L} \exp\left(\frac{-\Delta H_{LS}}{RT}\right) \quad (12)$$

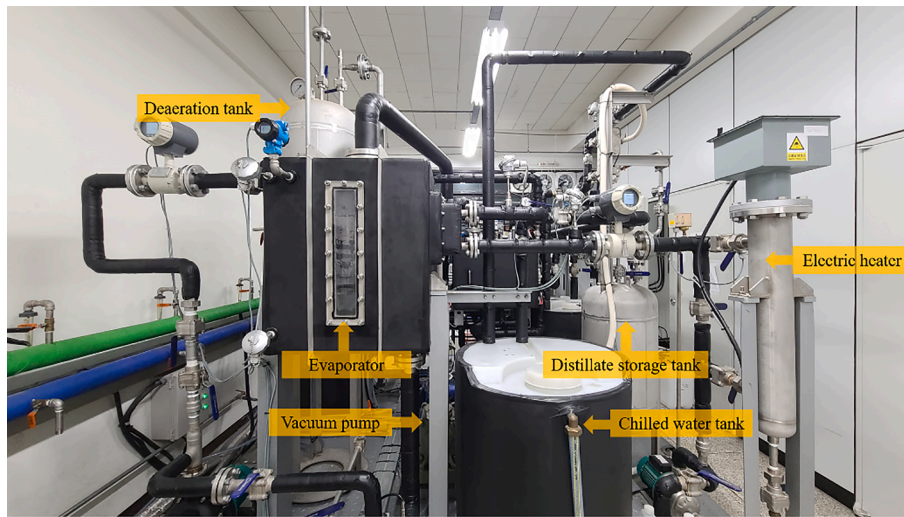
$$K_S = K_{0S} \exp\left(\frac{-\Delta H_{LS}}{RT}\right) \quad (13)$$

$$\theta = \theta_0 \exp\left(\frac{-\beta}{RT}\right) \quad (14)$$

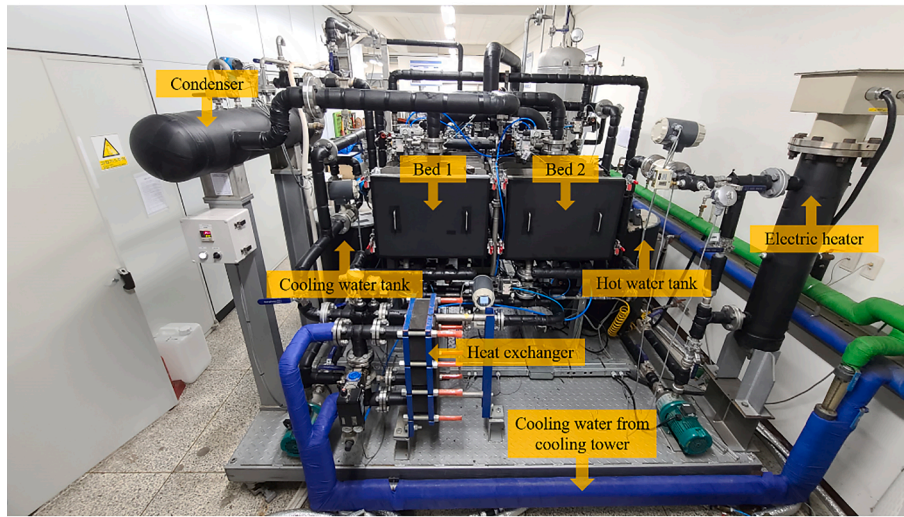
where q_{max} is the maximum water vapor uptake, K_L and K_S are the equilibrium constants, ΔH_{LS} is the isosteric enthalpy of adsorption, and θ is the adsorbent structural heterogeneity parameter.

3.2. Mathematical models of an AD cycle

The AD system consists primarily of an evaporator, a condenser, and two beds (i.e., adsorber and desorber), each containing fin-tube heat



(a)



(b)

Fig. 5. Pilot-scale (3 kW) two-bed AD system in Hanyang University, Republic of Korea: (a) front and (b) rear views.

exchangers filled with adsorbents. To evaluate the AD performance, a mathematical model was formulated using the mass and energy balance of major components such as the evaporator, condenser, adsorber, and desorber. The developed mathematical model was then validated through a comparison with the experimental results of a pilot-scale AD cycle using NS10 (Fig. 5). The assumptions for the development of the mathematical model were as follows: (i) a uniform temperature across the adsorbent layer, (ii) a uniform adsorption and desorption by the adsorbent, (iii) both the adsorbent (silica gel and zeolites) and gas phases of the adsorbate (water vapor) are in equilibrium condition, and (iv) heat loss to the environment is neglected.

The overall mass balance of the AD cycle is given by the following:

$$\frac{dM_{sw, evap}}{dt} = \dot{m}_{sw, in} - \dot{m}_{d, cond} - \dot{m}_{brine} \quad (15)$$

where $M_{sw, evap}$ is the mass of the seawater in the evaporator, $\dot{m}_{sw, in}$ is the mass flow rate of the feed seawater, $\dot{m}_{d, cond}$ is the distillate in the condenser, and \dot{m}_{brine} is the concentrated brine rejected from the evaporator.

The mass balance of salt in the evaporator of the AD cycle can be

expressed as follows:

$$M_{sw, evap} \frac{dX_{sw, evap}}{dt} = \dot{m}_{sw, in} X_{sw, in} - \dot{m}_{brine} X_{sw, evap} - x M_{ad} X_d \frac{dq_{ads}}{dt} \quad (16)$$

where $X_{sw, in}$ and $X_{sw, evap}$ are the concentrations of the feed and seawater in the evaporator, and X_d is the concentration of the water vapor.

The energy balance of the evaporator in communication with the adsorber is given as

$$\begin{aligned} & [M_{sw, evap} c_{p, sw} (T_{evap}, X_{evap}) + M_{HX, evap} c_{p, HX}] \frac{dT_{evap}}{dt} \\ & = \dot{m}_{sw, in} h_f (T_{evap}, X_{evap}) - x M_{ad} h_{fg} (T_{evap}) \left(\frac{dq_{ads}}{dt} \right) + \dot{m}_{chilled} c_{p, chilled} (T_{chilled, in} \\ & \quad - T_{chilled, out}) - \dot{m}_{brine} h_f (T_{evap}, X_{s, evap}) \end{aligned} \quad (17)$$

where $M_{HX, evap}$ is the thermal mass of the heat exchanger, M_{ad} is the mass of the adsorbent, and q_{ads} is the water vapor uptake by the adsorbent.

The energy balance of the adsorber and desorber is expressed as

$$\begin{aligned} & (M_{ad}c_{p,ad} + M_{HX,ads/des}c_{p,HX} + M_a c_{p,a}) \frac{dT_{ads/des}}{dt} \\ & = \pm x M_{ad} Q_{st}(T_{ads/des}, P_{evap/cond}) \frac{dq_{ads/des}}{dt} \pm \dot{m}_{cw/hw} c_{p,cw/hw}(T_{ads/des}) (T_{cw/hw,in} \\ & \quad - T_{cw/hw,out}) \end{aligned} \quad (18)$$

where Q_{st} and $c_{p,a}$ are the isosteric heat of adsorption and the specific heat of the adsorbed phase, respectively, and can be calculated using the following equations:

$$Q_{st} = h_{fg} + E \left\{ -\ln\left(\frac{q}{q_{max}}\right) \right\}^{1/\theta} + T v_g \left(\frac{\partial P}{\partial T} \right)_g \quad (19)$$

$$c_{p,a} = c_{p,g} + \left\{ \frac{1}{T} - \frac{1}{v_g} \left(\frac{\partial v_g}{\partial T} \right) \right\} Q_{st} - \frac{\partial Q_{st}}{\partial T} \Big|_P \quad (20)$$

The outlet temperature of the water from the heat exchanger was estimated using the log mean temperature difference method, which was determined from

$$T_{out} = T_0 + (T_{in} - T_0) \exp\left[\frac{-UA}{\dot{m}c_p(T_0)} \right] \quad (21)$$

where T_0 is the temperature of the heat exchanger.

The adsorption and desorption rates can be computed using the linear driving force (LDF) equation:

$$\frac{dq}{dt} = \frac{15D_{s0}e^{-\frac{E}{RT}}}{R_p^2} [q^* - q(t)] \quad (22)$$

where D_{s0} is the pre-exponential factor of the efficient water diffusivity, E is the activation energy, and R_p is the average radius of the adsorbent grains.

The energy balance of the condenser in communication with the desorber was expressed as follows:

$$\begin{aligned} & [M_{cond}c_p(T_{cond}) + M_{HX,cond}c_{p,HX}] \frac{dT_{cond}}{dt} \\ & = -x h_f(T_{cond}) \frac{dM_d}{dt} + M_{ad} h_{fg}(T_{cond}) \left(\frac{dq_{des}}{dt} \right) + \dot{m}_{condcw} c_{p,condcw} (T_{condcw,in} - T_{condcw,out}) \end{aligned} \quad (23)$$

where q_{des} is the amount of regenerated water vapor.

The rejected energy during the adsorption process and the energy required for the desorption process are given by the following:

$$Q_{ads} = \dot{m}_{cw} c_{p,cw}(T_{cw}) (T_{cw,out} - T_{cw,in}) \quad (24)$$

$$Q_{des} = \dot{m}_{hw} c_{p,hw}(T_{hw}) (T_{hw,in} - T_{hw,out}) \quad (25)$$

The heat transfer in the evaporator and condenser can be obtained through

$$Q_{evap} = \dot{m}_{chilled} c_{p,chilled}(T_{chilled}) (T_{chilled,in} - T_{chilled,out}) \quad (26)$$

and

$$Q_{cond} = \dot{m}_{cond} c_{p,condcw}(T_{condcw}) (T_{condcw,out} - T_{condcw,in}) \quad (27)$$

To evaluate the performance of the AD cycle, performance indexes (SDWP, SCC, COP, and PR) were used. The performance indexes were calculated using Eqs. (24)–(27):

$$SDWP = \frac{1}{t_{cycle}} \int_0^{t_{cycle}} \frac{Q_{cond} \tau}{h_{fg}(T_{cond}) M_{ad}} dt \quad (28)$$

$$SCC = \frac{1}{t_{cycle}} \int_0^{t_{cycle}} \frac{Q_{evap}}{M_{ad}} dt \quad (29)$$

$$COP = \frac{\int_0^{t_{cycle}} Q_{evap} dt}{\int_0^{t_{cycle}} Q_{des} dt} \quad (30)$$

$$PR = \frac{1}{t_{cycle}} \int_0^{t_{cycle}} \frac{\dot{M}_d h_{fg}(T_{cond})}{Q_{des}} dt \quad (31)$$

4. Results and discussion

4.1. Characteristics of physical properties

Fig. 6 shows the adsorption and desorption isotherms of the NS10 and FAM-Z series using nitrogen at 77 K and argon at 87 K, respectively. At extremely low relative pressures (i.e., $P/P_0 \approx 0$), all adsorbents showed a steep increase in the adsorbed volume by micropores. The knee of the isotherm where the monolayer adsorption was completed and multilayer adsorption began to occur was observed in all adsorbents at extremely low relative pressures (i.e., $P/P_0 \approx 0$). NS10 exhibited a notable hysteresis corresponding to capillary condensation, a typical characteristic of a mesoporous adsorbent; this corresponds to a type-IV isotherm model according to IUPAC [32]. By contrast, zeolites show a type-I isotherm, which is a typical characteristic of microporous materials [32]. The Brunauer–Emmett–Teller (BET) method was used to calculate the total surface area of the adsorbents. The micropores and external surface areas were then determined using the t-method proposed by de-Boer [33]. This procedure was identical to that implemented in the BET surface area measurement; however, the pressure range was extended to higher pressures to estimate the matrix or external surface area [33]. The pore volume, mean pore size, and pore size distribution were determined using the non-local density functional theory (NLDFT) method with a fitting error of 1.62% [34]. The cumulative pore volume and pore size distribution curves are shown in Fig. 7. The pore size distribution results clearly show that FAM-Z02 (i.e., CHA type) has a higher micropore distribution compared to other adsorbents (FAM-Z01, Z05, and NS10) [35]. Meanwhile, FAM-Z01 has brittle characteristics, which cause an interparticle void volume. Hence, relatively mesoporous characteristics were observed in comparison to other zeolites (i.e., FAM-Z02 and -Z05). The specific physical properties of the adsorbents calculated using the above methods are listed in Table 2.

4.2. Characteristics of water vapor uptakes

As shown in Fig. 8, water vapor uptake was investigated over a wide relative pressure range ($0 < P/P_0 < 0.8$) at temperatures between 20 °C and 80 °C, and the adsorption isotherms were plotted with respect to a partial pressure of below 12 kPa for a higher clarity of typical operating relative pressure ranges in the AD cycle.

At a low relative pressure (e.g., $P/P_0 < 0.3$, at a temperature of 80 °C), the equilibrium water adsorption on FAM-Z01 showed a hydrophobic characteristic from Henry's region (Fig. 8a), and the initial low adsorption can be considered from the perspective of nonpolar or weakly polar surface adsorption [13,15]. A sharp increase in water vapor uptake was then observed. This is because hydroxylation (e.g., Al–OH) and coordinative adsorption by chemical reactions can provide a sufficient number of hydrophilic sites, which can lead to anomalous isotherms (i.e., S-shape) [15]. That is, the initial low adsorption at an extremely low pressure is the threshold of the required water vapor uptake for chemical reactions [15]. The water adsorption isotherms of FAM-Z05 (Fig. 8c) were similar to those of FAM-Z01 (i.e., S-shape), described as a type-V isotherm. However, a longer hydrophobic length was observed because of the absence of Fe atoms, which have a relatively higher affinity for water than Al and P atoms [16]. Meanwhile, FAM-Z02 (Fig. 8b) exhibited very high adsorption and short hydrophobic length at low relative pressures (e.g., $P/P_0 < 0.2$, at a temperature of 80 °C) compared to AFI-type zeolites owing to its high micropore distribution (CHA type) [14,16,35]. In other words, Si atoms (FAM-

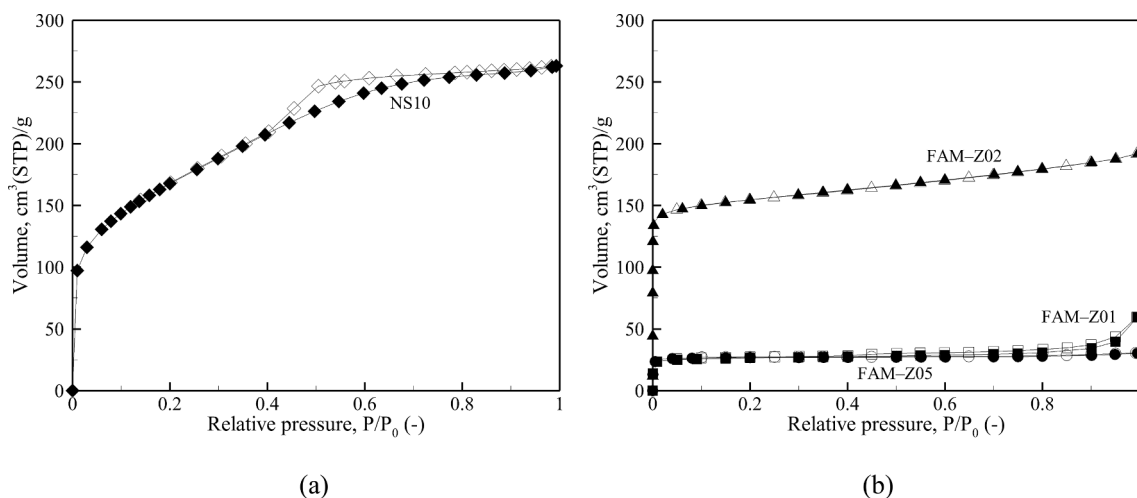


Fig. 6. Adsorption and desorption isotherms of (a) nitrogen at 77 K and (b) argon at 87 K. Filled and open symbols represent adsorption and desorption, respectively.

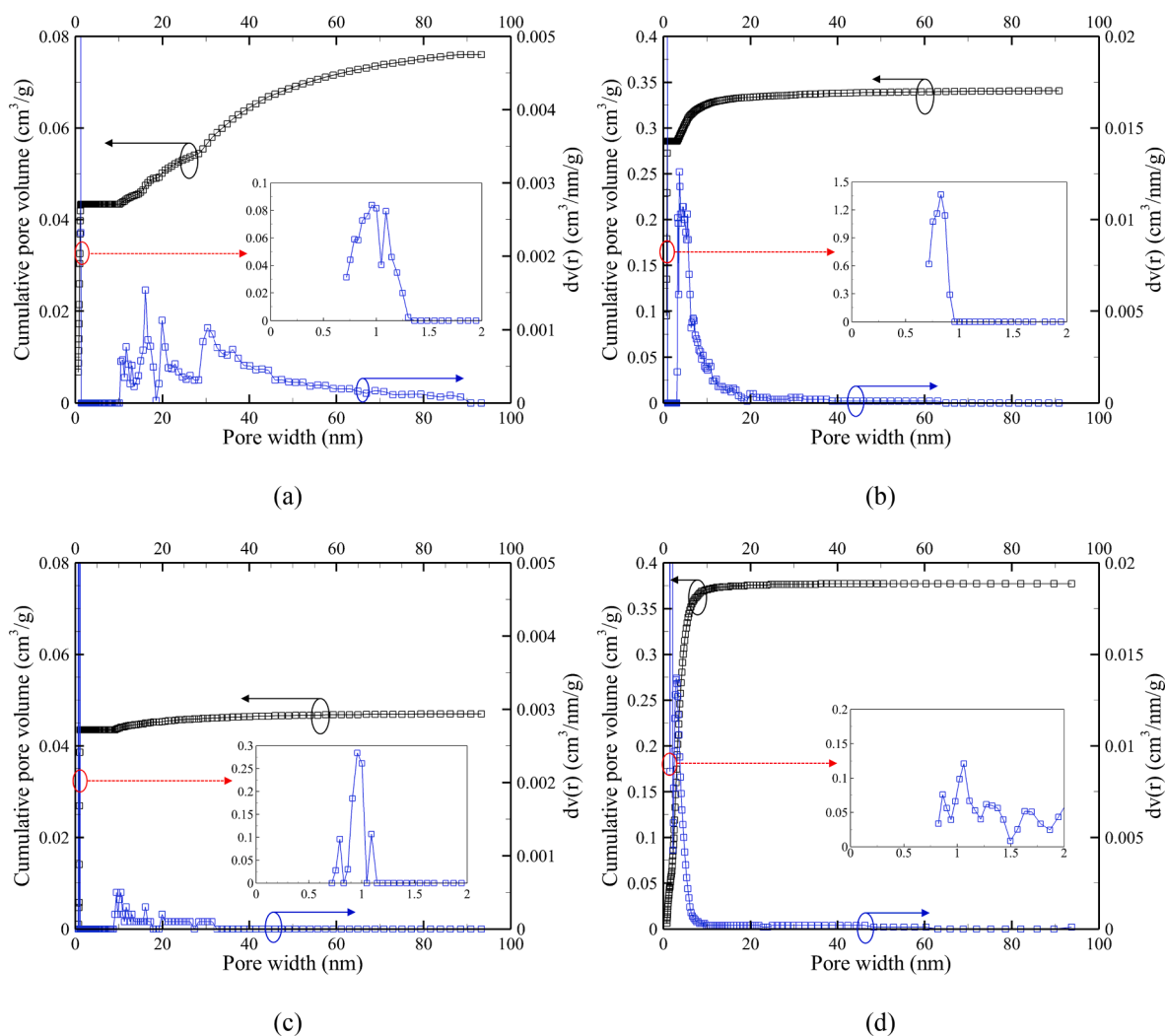


Fig. 7. Cumulative pore volume and pore size distribution curves of the zeolites and silica gel: (a) FAM-Z01, (b) FAM-Z02, (c) FAM-Z05, and (d) NS10.

Z02), which have a very high affinity for water molecules, form small pores (i.e., micropores) with the bonds of Al atoms, resulting in a stronger interaction between the adsorbate and the adsorbent [14,35]. An asymptotic increase in water vapor uptake was then observed in

FAM-Z02 because water molecules were gradually accommodated in larger pores where the adsorption affinity became weaker. Unlike AFI-type zeolites, which have a sigmoid adsorption isotherm, FAM-Z02 exhibited type-IV isotherms.

Table 2
Physical properties of the zeolites and silica gel.

| Parameters | FAM-Z01 | FAM-Z02 | FAM-Z05 | NS10 |
|---|---------|---------|---------|-------|
| Pore diameter (nm) | 0.978 | 0.830 | 0.958 | 2.33 |
| Pore volume (cm ³ /g) | 0.076 | 0.341 | 0.047 | 0.375 |
| Micropore volume (cm ³ /g) | 0.043 | 0.286 | 0.043 | 0.114 |
| BET surface area (m ² /g) | 91.8 | 536.7 | 97.2 | 586 |
| Micropore surface area (m ² /g) | 81.2 | 464.5 | 94.9 | 53 |
| External (non-micropore) surface area (m ² /g) | 10.6 | 72.2 | 2.3 | 533 |

NS10 (Fig. 8d) showed a marginally steep increase in the water vapor uptake by micropore filling at extremely low pressures ($P/P_0 \approx 0$), and the water vapor uptake was then increased linearly with monolayer and multilayer adsorption within the moderate pressure range ($0.05 < P/P_0 < 0.4$). A dramatic increase owing to capillary condensation, which is a typical feature of mesoporous adsorbents (i.e., type-IV isotherm) at high relative pressures ($0.4 < P/P_0 < 0.6$), and an asymptotic increase at such pressures ($P/P_0 > 0.6$) approaching the saturation pressure corresponding to the adsorbent temperature were sequentially observed.

4.3. Model verification

4.3.1. Adsorption isotherms

A linear plot of $\ln P$ versus $1/T$ with respect to water vapor uptake is illustrated in Fig. 9 to predict the isosteric enthalpy, which can be obtained from the slopes of the isosteric adsorption curves. The isosteric enthalpies (ΔH_s) for FAM-Z01 and Z05 were calculated at $q/q_m = 0.1$, where a sharp increase was observed through hydroxylation (e.g., Al–OH) and coordinative adsorption, as shown in Fig. 8 [16], while the isosteric enthalpies ($\Delta H_{I,S}$) for FAM-Z02 and NS10 was determined at $q/q_m = 0.5$ calculated using the Clausius–Clapeyron equation. The linear plot of $\ln K$ versus $1/T$ for the AFI-type zeolites is shown in Fig. 10. The isosteric enthalpies at zero coverage (ΔH_m) of FAM-Z01 and FAM-Z05 were 2773 and 2705 kJ/kg, respectively.

The parameters used in the adsorption isotherm models were calculated using the conjugate gradient method, which is a powerful iterative numerical technique for solving linear and nonlinear inverse problems of the parameter estimation [36]. The coefficient of determination (R^2), the most common objective function for the gradient descent algorithm, was used to assess the degree of fit between the adsorption isotherm model and the measured isotherm. The coefficient of determination can be calculated using the following equation:

$$R^2 = 1 - \frac{\sum_{i=1}^k (q_{meas,i} - \bar{q}_{calc,i})^2}{\sum_{i=1}^k (q_{meas,i} - \bar{q}_{meas})^2} \quad (32)$$

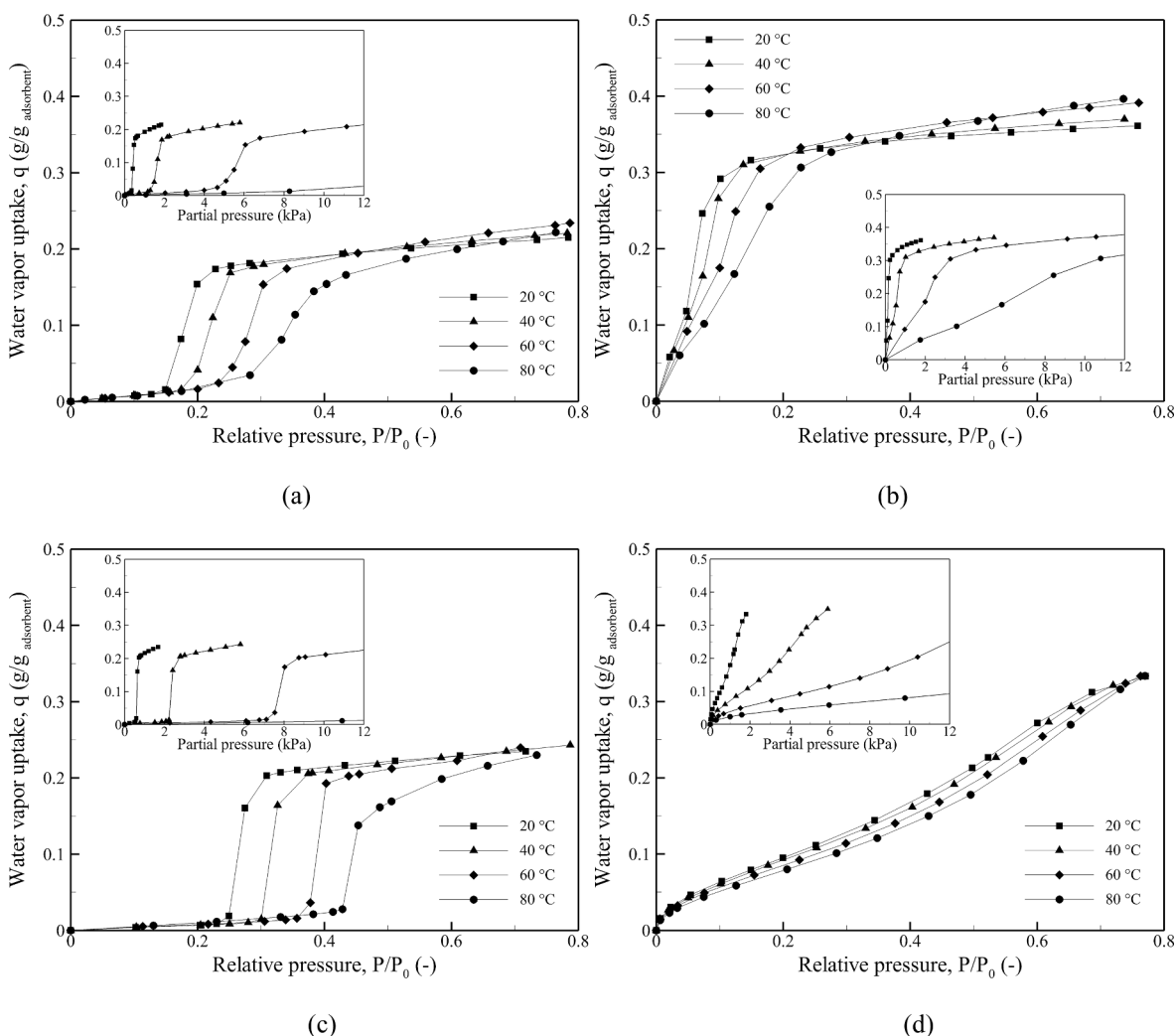


Fig. 8. Water vapor uptake of the adsorbents: (a) FAM-Z01, (b) FAM-Z02, (c) FAM-Z05, and (d) NS10. The square, triangular, diamond, and circular symbols denote the adsorbent temperatures of 20 °C, 40 °C, 60 °C, and 80 °C, respectively.

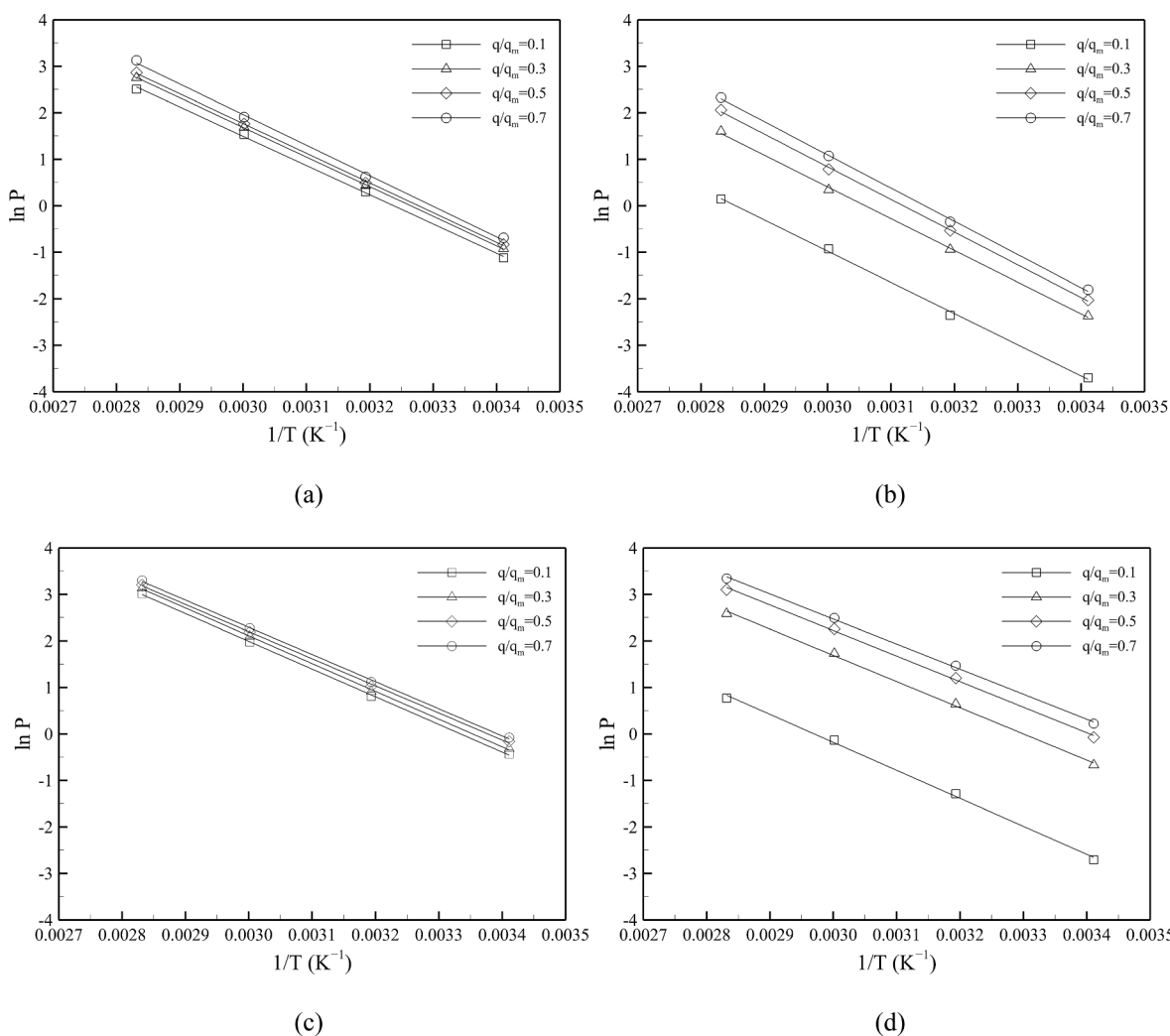


Fig. 9. Linear plot of $\ln P$ versus $1/T$ at different water vapor uptakes: (a) FAM-Z01, (b) FAM-Z02, (c) FAM-Z05, and (d) NS10.

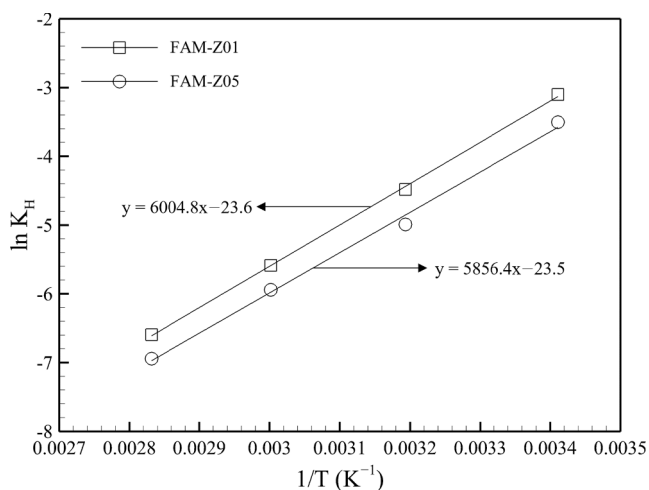


Fig. 10. Linear plot of $\ln K$ versus $1/T$ for FAM-Z01 and FAM-Z05.

with

$$\bar{q}_{meas} = \frac{1}{k} \sum_{i=1}^k q_{meas,i} \quad (33)$$

where k is the number of measured data.

Fig. 11 shows the equilibrium adsorption isotherm of water vapor on the adsorbents, where the symbols and solid lines represent the measured and predicted results (the modified Do-Do and hybrid Langmuir-Sips isotherms), respectively. For AFI-type zeolites, the modified Do-Do isotherm model can provide a good fit at a low relative pressure (i.e., Henry's region) and accurately capture the steep increase in the water vapor uptake by chemical reactions (i.e., hydroxylation and coordinative adsorption). Namely, the predicted results when using Eq. (1) with nine parameters (q_1 , α , K_{0s} , K_{0m} , ΔH_S , ΔH_M , N , q_2 , and β), as shown in Table 3, showed a reasonable agreement with the measured data over a pressure ranging from 0 to 12 kPa at a temperature of 20 °C to 80 °C. Here, seven parameters (q_1 , α , K_{0s} , K_{0m} , N , q_2 , β) were regressed to fit the measured adsorption isotherms using the conjugate gradient method, and isosteric enthalpy (ΔH_S and ΔH_M) was calculated using Clausius-Clapeyron and Henry's equations, respectively. The R-squared values of the modified Do-Do isotherm model were 0.984 (FAM-Z01) and 0.986 (FAM-Z05), respectively. The hybrid Langmuir-Sips isotherm model using the isosteric enthalpy (ΔH_{LS}) calculated through the Clausius-Clapeyron equation and five regression parameters (α , K_{0L} , K_{0S} , θ_0 , and β) has been shown to accurately capture the adsorption isotherms of CHA-type zeolites. The model can replicate the high adsorption capacity owing to the presence of Si atoms at low pressure using the Langmuir isotherm model and the asymptotic increase in water vapor uptake occurring from multilayer adsorption at moderate pressure when using

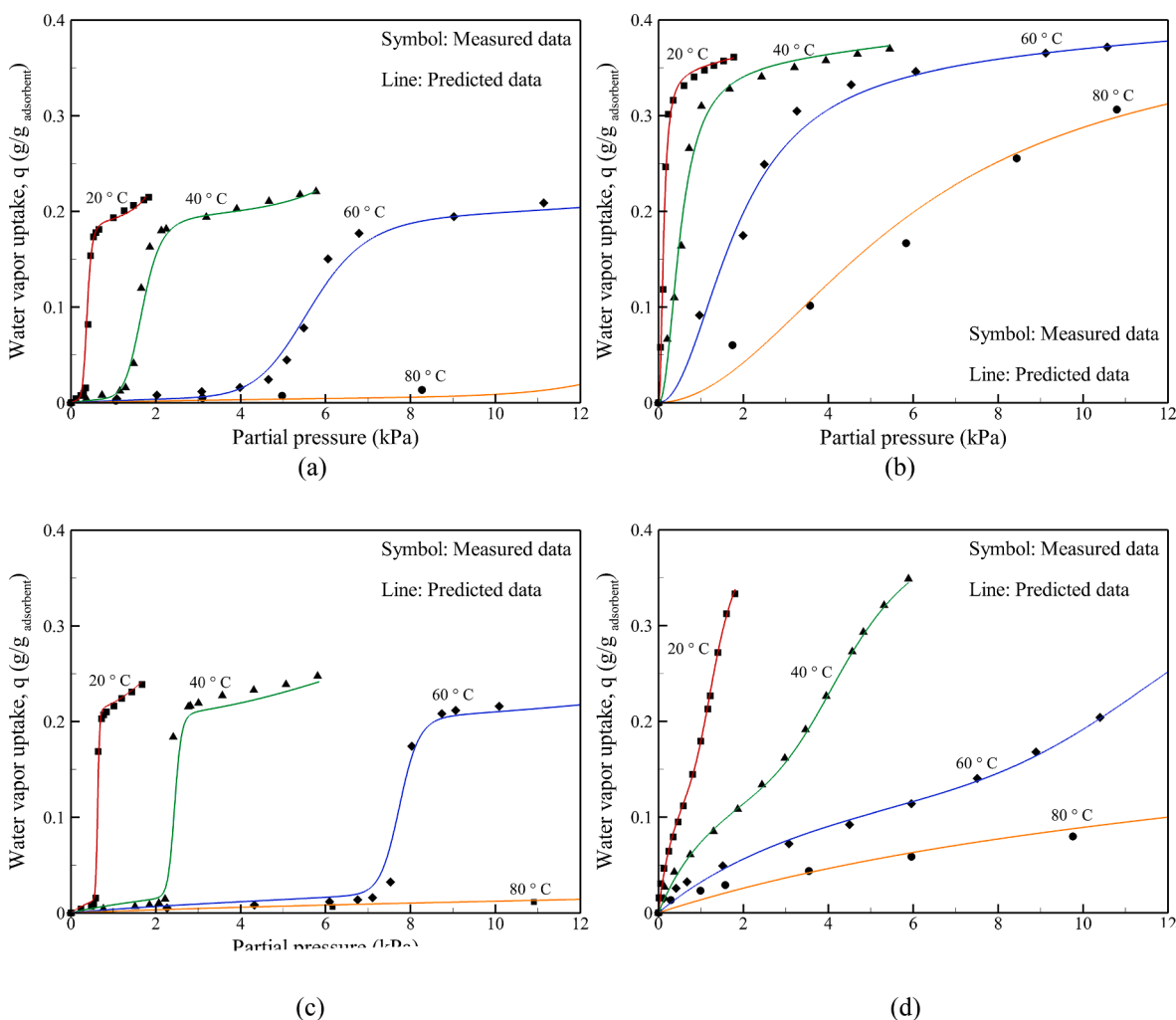


Fig. 11. Equilibrium adsorption isotherm of water vapor on (a) FAM-Z01, (b) FAM-Z02, (c) FAM-Z05, and (d) NS10. The symbols and lines denote the measured and predicted results (modified Do-Do isotherm model for FAM-Z01 and Z05 and hybrid Langmuir-Sips isotherm model for FAM-Z02 and NS10), respectively.

the Sips isotherm. The model is also applicable for describing the equilibrium adsorption isotherm of a silica gel (i.e., mesoporous adsorbent) such as micropore filling, monolayer and multilayer adsorption, and capillary condensation. The R-squared values of the hybrid Langmuir-Sips isotherm model were 0.990 (FAM-Z02) and 0.998 (NS10), respectively. Therefore, the two proposed models are capable of covering the adsorption characteristics of water vapor on the adsorbents over the expected working pressure ranges in the AD cycle.

4.3.2. AD cycle

The temporal pressure profiles in the AD cycle using NS10 and SDWP were investigated under specific operating conditions (Fig. 12), and the hot, cooling, and chilled water temperatures were maintained at 80 °C, 25 °C, and 20 °C, respectively, and the other parameters used in the simulation are as described in Table 4. The AD system was batch-operated concomitantly with the adsorption-triggered-evaporation and desorption-activated-condensation processes. The vapor pressure is increased (adsorber) and decreased (desorber) during the pre-heating and cooling modes for the transition to the desorption and adsorption processes, respectively, and the pressure profile agrees well with that of the experimental results (Fig. 12a). Meanwhile, the SDWP decreased at a relatively short cycle time because the desorption process had not been sufficiently completed, and a low SDWP was also observed at a relatively longer cycle time owing to a high adsorption rate at the beginning [3,37]. The predicted SDWP also showed good agreement with the

experimental results, within a maximum relative deviation of 2.3% (Fig. 12b).

4.4. Performance evaluation

It is widely known that the silica gel and MOFs show the limited performance and applicability for the AD cycle because of their low net equilibrium adsorption capacity and weakness for water, respectively. In this study, the AD performance of commercial zeolites (i.e., FAM-Z series with AFI and CHA types) was investigated with respect to the key parameters (i.e., hot- and chilled-water temperatures). To investigate the possibility of using zeolite as an adsorbent in the AD cycle, the AD performance using the FAM-Z series was compared with that using silica gel. This applicability was also investigated for the potential application of the AD cycle powered by the extremely low-grade waste heat (e.g., 55 °C) commonly found in industrial plants and solar energy.

The effect of the hot-water temperature on the performance was investigated (Fig. 13); here, the other parameters remained constant ($T_{chilled,in} = 20$ °C, $T_{cw,in} = 25$ °C, and $t_{half-cycle} = 636$ s). The results revealed that the AD performance (i.e., SDWP, SCC, COP, and PR) increased with the hot-water temperature for the zeolites. The saturation vapor pressure (P_0) corresponding to the adsorbent temperature increased as the hot-water temperature increased, resulting in a low relative pressure (P_{des}/P_0) during the desorption process [3,17]. Hence, the equilibrium water vapor uptake decreased during the desorption

Table 3
Modified Do-Do and hybrid Langmuir-Sips isotherm models for water vapor adsorption on FAM-Z series and silica gel.

| Isotherm model | Adsorbent | Parameters | Values |
|-------------------------------------|-----------|-------------------------|------------------------|
| Modified Do-Do isotherm model | FAM-Z01 | q_1 (g/g) | 2.733×10^{-2} |
| | | α (J/mol) | 2.967×10^3 |
| | | $\ln(K_{0s})$ | 4.514×10^4 |
| | | $\ln(K_{0m})$ | 5.126×10^4 |
| | | ΔH_s (J/mol) | -5.201×10^4 |
| | | ΔH_m (J/mol) | -4.991×10^4 |
| | | N | 17 |
| | | M | 8 |
| | | q_2 (g/g) | 1.32×10^{-1} |
| | | β (J/mol) | 8.575×10^2 |
| | R^2 | 0.984 | |
| | FAM-Z05 | q_1 (g/g) | 2.001×10^{-2} |
| | | α (J/mol) | -12.967 |
| | | $\ln(K_{0s})$ | 4.954×10^4 |
| | | $\ln(K_{0m})$ | 8.242×10^3 |
| | | ΔH_s (J/mol) | -4.933×10^4 |
| | | ΔH_m (J/mol) | -4.869×10^4 |
| | | N | 28 |
| | | M | 10 |
| | | q_2 (g/g) | 2.294×10^{-1} |
| β (J/mol) | | 16.599 | |
| R^2 | 0.986 | | |
| Hybrid Langmuir-Sips isotherm model | FAM-Z02 | q_{max} (g/g) | 0.423 |
| | | α (J/mol) | 5.267×10^3 |
| | | $\ln(K_{0L})$ | 6.933×10^4 |
| | | $\ln(K_{0S})$ | 4.779×10^4 |
| | | ΔH_{LS} (J/mol) | -5.821×10^4 |
| | | θ_0 | 6.212 |
| | | β (J/mol) | 2.853×10^3 |
| | R^2 | 0.990 | |
| | NS10 | q_{max} (g/g) | 0.339 |
| | | α (J/mol) | 1.375×10^3 |
| | | $\ln(K_{0L})$ | 4.169×10^4 |
| | | $\ln(K_{0S})$ | 4.602×10^4 |
| | | ΔH_{LS} (J/mol) | -4.716×10^4 |
| | | θ_0 | 18.520 |
| β (J/mol) | | 3.322×10^3 | |
| R^2 | 0.998 | | |

process, and thus an increase in the net equilibrium adsorption capacity (i.e., increase in the performance) was observed as the hot-water temperature increased [3,17]. However, AFI-type zeolites have inflection temperature points where the performance (especially COP and PR) deteriorates at temperatures ranging from 55 °C to 65 °C. This is because

as hot-water temperature increases (>65 °C), the increase in heat consumed during the desorption process is much greater than the increase in cooling capacity and freshwater production caused by the increase in net equilibrium adsorption capacity owing to the nature of S-shape isotherms [17]. In contrast, nearly consistent performance (i.e., SDWP and SCC) was observed at hot-water temperatures (>65 °C) owing to the adsorption characteristics dominated by the Henry's region ($P/P_0 < 0.2$) [17]. Consequently, the results indicate that AFI-type zeolites can be efficiently regenerated through a low-grade heat source in the desorption process owing to their unusual isotherms (i.e., S-shape). Among the AFI-type zeolites, FAM-Z05 showed a relatively high performance compared to other adsorbents at extremely low regeneration temperatures (<62 °C) because the relatively long hydrophobic length owing to the absence of FeO₄ can result in a low adsorption capacity at low regeneration temperatures. Meanwhile, a steep increase in the performance of the CHA-type was represented with respect to the hot-water temperature because the adsorption capacity during the desorption process decreased dramatically with an increase in the regeneration temperature owing to the CHA-type structure; that is, the large number of small pores (i.e., micropores) formed by the bonds of Si and Al atoms cause a short hydrophobic length and a steep increase in adsorption capacity at low relative pressures ($P/P_0 < 0.2$), resulting in a high net

Table 4
Operating conditions of the two-bed AD cycle.

| | | |
|-----------------------------------|---------------------------------|--------|
| Mass | $M_{adsorbent}$ (kg) | 28 |
| | M_{cond} (kg) | 2 |
| | M_{evap} (kg) | 66 |
| Thermal mass | $M_{HX,ads/des}C_{p,HX}$ (kg/K) | 144.70 |
| | $M_{HX,evap}C_{p,HX}$ (kg/K) | 42.82 |
| | $M_{HX,cond}C_{p,HX}$ (kg/K) | 38.6 |
| Overall heat transfer coefficient | U_{ads} (W/m ² K) | 250 |
| | U_{des} (W/m ² K) | 240 |
| | U_{evap} (W/m ² K) | 1715 |
| | U_{cond} (W/m ² K) | 2658 |
| Heat transfer area | A_{evap} (m ²) | 0.79 |
| | A_{cond} (m ²) | 1.56 |
| | $A_{ads/des}$ (m ²) | 19.72 |
| Mass flow rate | $\dot{m}_{chilled}$ (kg/s) | 0.28 |
| | \dot{m}_{condcw} (kg/s) | 0.60 |
| | \dot{m}_{cw} (kg/s) | 0.57 |
| | \dot{m}_{hw} (kg/s) | 0.67 |
| Temperature | $T_{cw,in}$ (°C) | 25 |
| | $T_{chilled,in}$ (°C) | 20 |
| | $T_{hot,in}$ (°C) | 80 |

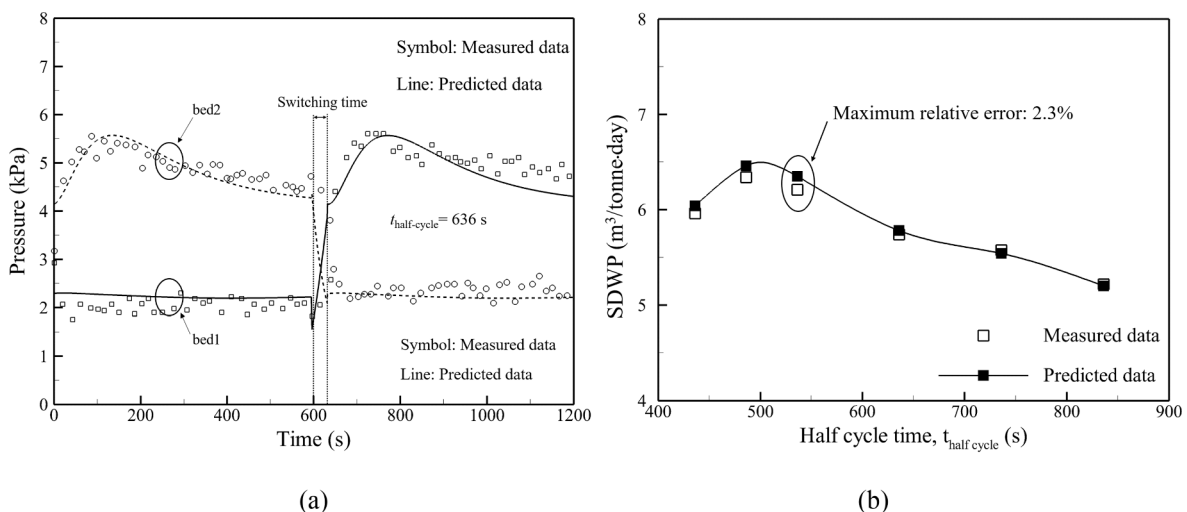


Fig. 12. (a) Temporal pressure profile in adsorber and desorber and (b) SDWP with respect to cycle time ($T_{hot,in} = 80$ °C, $T_{cw,in} = 25$ °C, $T_{chilled,in} = 20$ °C, and $t_{half-cycle} = 636$ s).

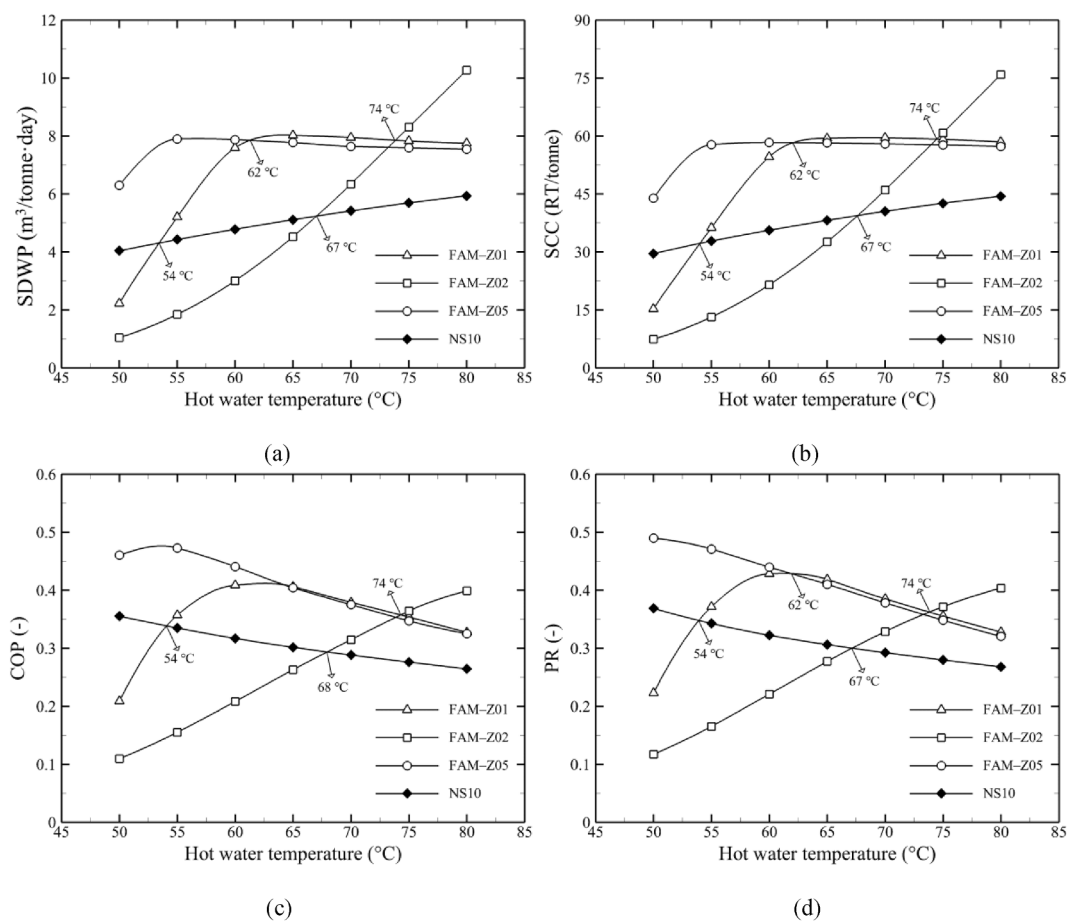


Fig. 13. (a) SDWP, (b) SCC, (c) COP, and (d) PR with respect to hot-water temperature ($T_{hot,in} = 50\text{ }^{\circ}\text{C}$ to $80\text{ }^{\circ}\text{C}$, $T_{cw,in} = 25\text{ }^{\circ}\text{C}$, $T_{chilled,in} = 20\text{ }^{\circ}\text{C}$, and $t_{half-cycle} = 636\text{ s}$). The triangle, square, circle, and diamond symbols represent the FAM-Z01, FAM-Z02, FAM-Z05, and NS10, respectively.

equilibrium adsorption capacity (i.e., high performance) at high hot-water temperatures ($>74\text{ }^{\circ}\text{C}$). NS10 also showed that SDWP and SCC increased with an increase in the hot-water temperature, but the COP and PR decreased with hot-water temperature. This is because the increase in heat consumed during the desorption process is much greater than the increase in cooling capacity owing to the linear increase in net equilibrium adsorption capacity [38].

As a result, FAM-Z01 is superior to FAM-Z02 and silica gel within the temperature range of $54\text{ }^{\circ}\text{C}$ to $74\text{ }^{\circ}\text{C}$, whereas FAM-Z02 is advantageous for AD cycles using relatively high regeneration temperatures ($>74\text{ }^{\circ}\text{C}$). Meanwhile, FAM-Z05 showed a relatively high performance compared to other adsorbents, demonstrating its potential as an adsorbent for AD cycles driven by an extremely low-grade heat source (i.e., $T_{hot,in} < 55\text{ }^{\circ}\text{C}$). Consequently, AFI- and CHA-type zeolites are promising adsorbents for adsorption desalination and cooling systems with low-grade and high-grade heat sources, respectively. Here, the maximum performance of the FAM-Z series (SDWP, SCC, COP, and PR, respectively) was as follows: $8.13\text{ m}^3/\text{tonne}\cdot\text{day}$, $59.56\text{ RT}/\text{tonne}$, 0.41 , and 0.43 (FAM-Z01); $10.27\text{ m}^3/\text{tonne}\cdot\text{day}$, $75.87\text{ RT}/\text{tonne}$, 0.40 , and 0.40 (FAM-Z02); and $7.89\text{ m}^3/\text{tonne}\cdot\text{day}$, $58.33\text{ RT}/\text{tonne}$, 0.47 , and 0.49 (FAM-Z05) under the specified operating conditions.

The influence of chilled-water temperature ranging from $10\text{ }^{\circ}\text{C}$ to $30\text{ }^{\circ}\text{C}$ on AD performance was identified (Fig. 14). The other parameters remained constant ($T_{hot,in} = 55\text{ }^{\circ}\text{C}$, $T_{cw,in} = 25\text{ }^{\circ}\text{C}$, and $t_{half-cycle} = 636\text{ s}$), and the specific operating conditions used in the simulation are as listed in Table 4. The results indicate that the performance (i.e., SDWP, SCC, COP, and PR) increased with an increase in the chilled water temperature. This is because the vapor pressure in the evaporator ($P_{ads} \approx P_{evap}$) increased with an increase in the chilled water temperature, which in

turn resulted in an increase in the relative pressure (P_{ads}/P_0) during the adsorption process, and consequently increased the net equilibrium adsorption capacity (Δq) [3,39]. In addition, although relatively large amounts of water vapor were desorbed, the water vapor pressure of the desorber (P_{des}/P_0) increased slightly because the saturation vapor pressure (P_0) corresponding to the temperature of the adsorbent was considerably high. However, the AD performance was relatively insensitive to the chilled-water temperature for FAM-Z01. This is because the water vapor uptake gradient ($\Delta q/\Delta P$) with respect to the vapor pressure is nearly consistent with the adsorption ($\Delta q_{ads}/\Delta P_{ads}$) and desorption ($\Delta q_{des}/\Delta P_{des}$) process owing to the relatively short hydrophobic length (Fig. 8a). Meanwhile, a relatively rapid improvement in the performance was observed in FAM-Z05 and NS10 with respect to the chilled-water temperature. This is because a steep increase in the adsorption capacity of FAM-Z05, attributed to a relatively longer hydrophobic length, and a rapid increase in the adsorption capacity of NS10 caused by multilayer adsorption and capillary condensation were observed during the adsorption process (Fig. 8c and 8d). Although FAM-Z02 showed linear performance improvements over a wide range of chilled-water temperatures, it demonstrated the lowest performance owing to the extremely high energy required for desorption [40]. For low-grade heat sources ($T_{hot,in} = 55\text{ }^{\circ}\text{C}$), FAM-Z05 is superior to FAM-Z02 and NS10 because of its high net equilibrium adsorption capacity owing to the relatively long hydrophobic length of the sigmoid adsorption isotherm. Meanwhile, FAM-Z01 showed a relatively higher performance than FAM-Z05 at low chilled water temperatures ($T_{chilled,in} < 13\text{ }^{\circ}\text{C}$) because it has a short hydrophobic length and can induce a high adsorption capacity during the adsorption process. Consequently, AFI-type zeolites showed that FAM-Z01 and -Z05 can be used for district

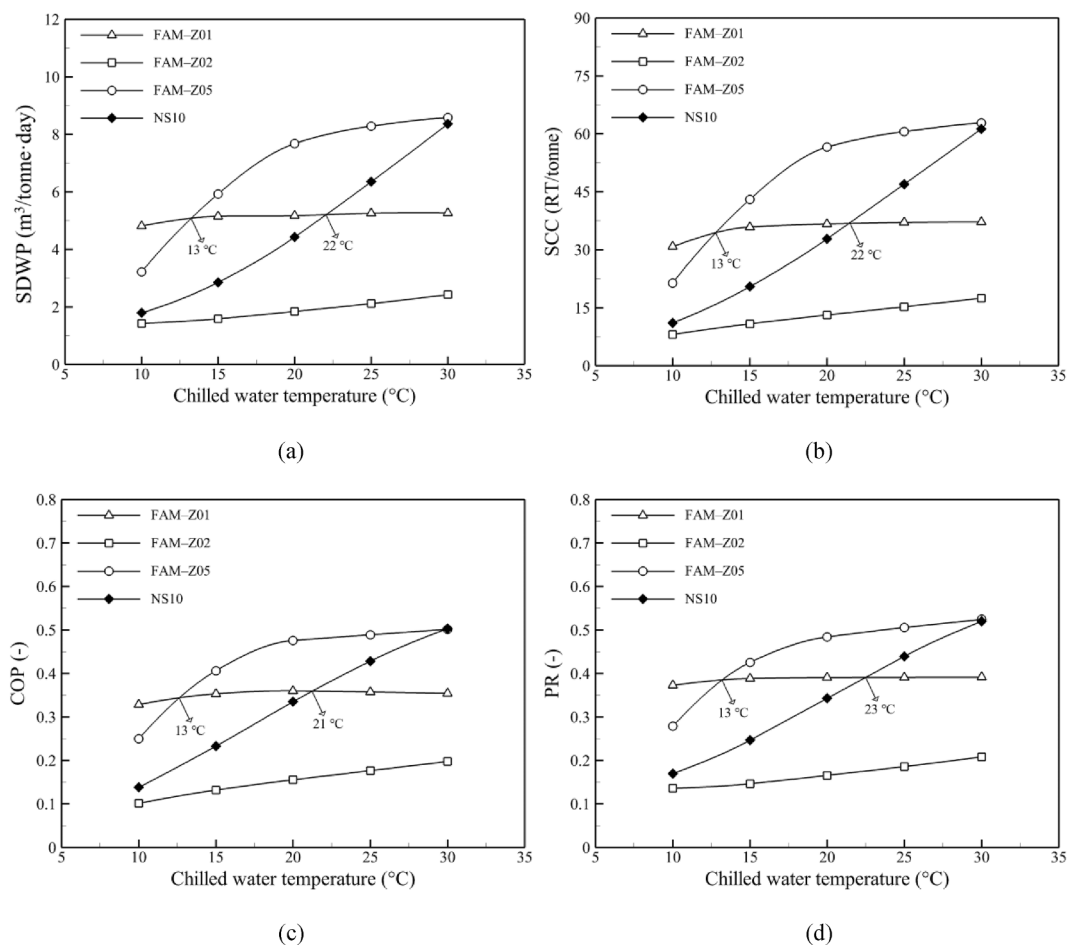


Fig. 14. The effects of the chilled water temperature on the (a) SDWP, (b) SCC, (c) COP, and PR ($T_{hot,in} = 55\text{ }^{\circ}\text{C}$, $T_{cw,in} = 25\text{ }^{\circ}\text{C}$, $T_{chilled,in} = 10\text{ }^{\circ}\text{C}$ to $30\text{ }^{\circ}\text{C}$, and $t_{half-cycle} = 636\text{ s}$). The triangle, square, circle, and diamond symbols represent the FAM-Z01, FAM-Z02, FAM-Z05, and NS10, respectively.

cooling ($T_{chilled,in} > 13\text{ }^{\circ}\text{C}$) and residential space cooling ($T_{chilled,in} < 13\text{ }^{\circ}\text{C}$) with low-grade heat sources ($T_{hot,in} = 55\text{ }^{\circ}\text{C}$), respectively [3]. The highest performance of the zeolites (SDWP, SCC, COP, and PR, respectively) was as follows under specific operating conditions of $5.27\text{ m}^3/\text{tonne-day}$, 37.22 RT/tonne , 0.36 , and 0.39 (FAM-Z01); $2.43\text{ m}^3/\text{tonne-day}$, 17.50 RT/tonne , 0.20 , and 0.21 (FAM-Z02); and $8.58\text{ m}^3/\text{tonne-day}$, 62.82 RT/tonne , 0.50 , and 0.52 (FAM-Z05).

Fig. 15 shows the performance (i.e., SDWP and COP) of the AD cycle over the cycle time ($t_{half-cycle} = 136$ to 736 s) using a low-grade heat source ($T_{hot,in} = 55\text{ }^{\circ}\text{C}$ to $65\text{ }^{\circ}\text{C}$); here, the other parameters remained constant ($T_{chilled,in} = 20\text{ }^{\circ}\text{C}$ and $T_{cw,in} = 25\text{ }^{\circ}\text{C}$). It was noted that relatively low SDWP was observed for all adsorbents at relatively short and long cycle times owing to the insufficient and excessive desorption process. In addition, as the hot-water temperature increased, the kinetic energy of the water vapor trapped in the adsorbent pores reached the threshold kinetic energy more rapidly, slightly reducing the cycle time at which maximum SDWP was achieved (NS10, FAM-Z01 and -Z02) [3]. In contrast, FAM-Z05 showed that the cycle time to achieve maximum SDWP increases with increasing hot-water temperature. Despite the low regeneration temperature of FAM-Z05 ($< 55\text{ }^{\circ}\text{C}$), increasing the regeneration temperature slightly increases the net equilibrium adsorption capacity and increases the residual thermal energy from the previous desorption process; this will slightly increase the cycle time required to remove it. Meanwhile, COP asymptotically increases with cycle time; this is because, with increasing cycle time, the linear increase in heat of desorption is less than the asymptotic increase in the cooling capacity of all adsorbents.

5. Conclusions

This paper presents detailed experimental and theoretical approaches for the assessment of the applicability of the functional adsorption material zeolite (i.e., FAM-Z series) for adsorption desalination cum cooling systems, and the following results were achieved.

- The modified Do-Do and hybrid Langmuir-Sips isotherm models were proposed to satisfactorily fit anomalous stepwise isotherms of the FAM-Z series and the adsorption isotherms of silica gel with mesoporous adsorption characteristics. The parameters used in the isotherm model were regressed using the conjugate gradient method, and the isosteric enthalpy was calculated using the Clausius-Clapeyron and Henry equations. The coefficient of determination (R^2) was observed to be above 0.984, indicating that the proposed isotherm models showed consistency with the measured isotherm data. The mathematical model was formulated to evaluate the AD performance, and the model results exhibited good agreement with the experimental results; here, a maximum relative error of approximately 2.3% in terms of SDWP was shown.
- The results revealed that AFI- and CHA-type zeolites were advantageous for adsorption desalination and cooling systems with low-grade and high-grade ($> 74\text{ }^{\circ}\text{C}$) heat sources, respectively. FAM-Z05 exhibited a relatively high performance compared to other adsorbents owing to its relatively long hydrophobic length of the sigmoid adsorption isotherm, demonstrating its high potential as an adsorbent for AD cycles driven by extremely low-grade heat sources ($< 55\text{ }^{\circ}\text{C}$). In addition, FAM-Z01 and Z05 showed the applicability of

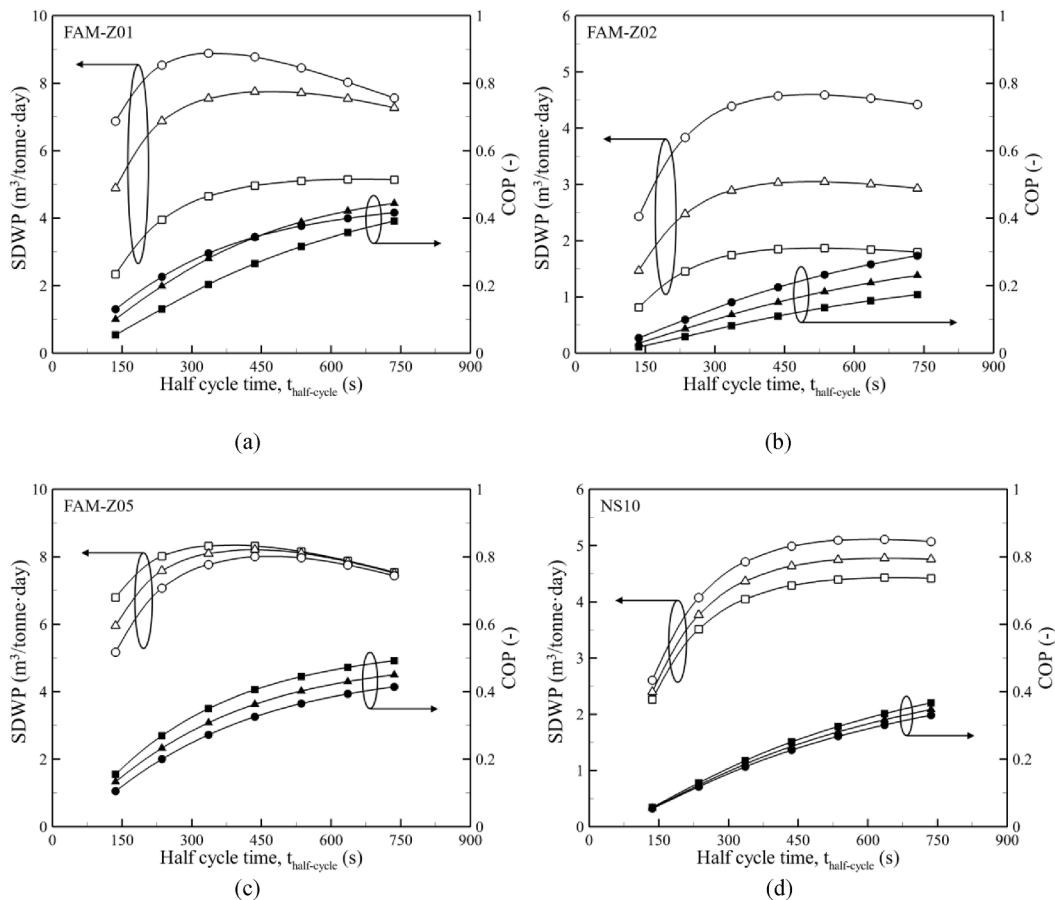


Fig. 15. SDWP and COP of AD cycles using (a) FAM-Z01, (b) FAM-Z02, (c) FAM-Z05, and (d) NS10 with respect to hot-water temperature and cycle time ($T_{ho, in} = 55\text{ }^{\circ}\text{C}$ to $65\text{ }^{\circ}\text{C}$, $T_{cw, in} = 25\text{ }^{\circ}\text{C}$, $T_{chilled, in} = 20\text{ }^{\circ}\text{C}$, and $t_{half-cycle} = 136$ to 736 s). The open and filled symbols represent the SDWP and COP, respectively, and the square, triangle, and circle symbols represent $55\text{ }^{\circ}\text{C}$, $60\text{ }^{\circ}\text{C}$, and $65\text{ }^{\circ}\text{C}$, respectively.

district cooling ($T_{chilled, in} > 13\text{ }^{\circ}\text{C}$) and residential cooling ($T_{chilled, in} < 13\text{ }^{\circ}\text{C}$) with low-grade heat sources ($T_{hot, in} = 55\text{ }^{\circ}\text{C}$), respectively.

Declaration of Competing Interest

The authors declare that they have no known competing financial interests or personal relationships that could have appeared to influence the work reported in this paper.

Acknowledgments

This research was supported by a grant from the Endowment Project of “Development of Seawater Desalination-Cooling Plant using Unutilized Energy (3/5)” funded by the Korea Research Institute of Ships and Ocean Engineering (PES3970).

References

- [1] Y.-D. Kim, K. Thu, K.C. Ng, G.L. Amy, N. Ghaffour, A novel integrated thermal-membrane-based solar energy-driven hybrid desalination system: Concept description and simulation results, *Water Res.* 100 (2016) 7–19.
- [2] J.W. Wu, M.J. Biggs, P. Pendleton, A. Badalyan, E.J. Hu, Experimental implementation and validation of thermodynamic cycles of adsorption-based desalination, *Appl. Energy* 98 (2012) 190–197.
- [3] S.-Y. Woo, H.-S. Lee, H. Ji, D.-S. Moon, Y.-D. Kim, Silica gel-based adsorption cooling cum desalination system: Focus on brine salinity, operating pressure, and its effect on performance, *Desalination* 467 (2019) 136–146.
- [4] R.H. Mohammed, O. Mesalhy, M.L. Elsayed, M. Su, L.C. Chow, Revisiting the adsorption equilibrium equations of silica-gel/water for adsorption cooling applications, *Int. J. Refrig* 86 (2018) 40–47.
- [5] A.R.M. Rezk, R.K. Al-Dadah, Physical and operating conditions effects on silica gel/water adsorption chiller performance, *Appl. Energy* 89 (1) (2012) 142–149.
- [6] P.J. Vodanitskaia, J.J. Soares, H. Melo, J.M. Gurgel, Experimental chiller with silica gel: Adsorption kinetics analysis and performance evaluation, *Energy Convers. Manage.* 132 (2017) 172–179.
- [7] E. Elsayed, R. Al-Dadah, S. Mahmoud, P. Anderson, A. Elsayed, Experimental testing of aluminium fumarate MOF for adsorption desalination, *Desalination* 475 (2020), 114170.
- [8] E. Elsayed, R. Al-Dadah, S. Mahmoud, P.A. Anderson, A. Elsayed, P.G. Youssef, CPO-27(Ni), aluminium fumarate and MIL-101(Cr) MOF materials for adsorption water desalination, *Desalination* 406 (2017) 25–36.
- [9] E. Elsayed, P. Anderson, R. Al-Dadah, S. Mahmoud, A. Elsayed, MIL-101(Cr)/calcium chloride composites for enhanced adsorption cooling and water desalination, *J. Solid State Chem.* 277 (2019) 123–132.
- [10] H.J. An, M. Sarker, D.K. Yoo, S.H. Jhung, Water adsorption/desorption over metal-organic frameworks with ammonium group for possible application in adsorption heat transformation, *Chem. Eng. J.* 373 (2019) 1064–1071.
- [11] S.M. Ali, A. Chakraborty, Adsorption assisted double stage cooling and desalination employing silica gel+water and AQSOA-Z02+water systems, *Energy Convers. Manage.* 117 (2016) 193–205.
- [12] W.u. Fan, A. Chakraborty, Isothermic heat of adsorption at zero coverage for AQSOA-Z01/Z02/Z05 zeolites and water systems, *Microporous Mesoporous Mater.* 260 (2018) 201–207.
- [13] S.W. Hong, S.H. Ahn, J.D. Chung, K.J. Bae, D.A. Cha, O.K. Kwon, Characteristics of FAM-Z01 compared to silica gels in the performance of an adsorption bed, *Appl. Therm. Eng.* 104 (2016) 24–33.
- [14] S. Kayal, S. Baichuan, B.B. Saha, Adsorption characteristics of AQSOA zeolites and water for adsorption chillers, *Int. J. Heat Mass Transf.* 92 (2016) 1120–1127.
- [15] Y.-D. Kim, K. Thu, K.C. Ng, Adsorption characteristics of water vapor on ferroaluminophosphate for desalination cycle, *Desalination* 344 (2014) 350–356.
- [16] H. Wei Benjamin Teo, A. Chakraborty, W. Fan, Improved adsorption characteristics data for AQSOA types zeolites and water systems under static and dynamic conditions, *Microporous Mesoporous Mater.* 242 (2017) 109–117.
- [17] H.W.B. Teo, A. Chakraborty, B. Han, Water adsorption on CHA and AFI types zeolites: modelling and investigation of adsorption chiller under static and dynamic conditions, *Appl. Therm. Eng.* 127 (2017) 35–45.

- [18] K.C. Ng, K. Thu, Y. Kim, A. Chakraborty, G. Amy, Adsorption desalination: An emerging low-cost thermal desalination method, *Desalination* 308 (2013) 161–179.
- [19] A. Li, A.B. Ismail, K. Thu, K.C. Ng, W.S. Loh, Performance evaluation of a zeolite–water adsorption chiller with entropy analysis of thermodynamic insight, *Appl. Energy* 130 (2014) 702–711.
- [20] P.G. Youssef, S.M. Mahmoud, R.K. AL-Dadah, Performance analysis of four bed adsorption water desalination/refrigeration system, comparison of AQSOA-Z02 to silica-gel, *Desalination* 375 (2015) 100–107.
- [21] P.G. Youssef, S.M. Mahmoud, R.K. AL-Dadah, Numerical simulation of combined adsorption desalination and cooling cycles with integrated evaporator/condenser, *Desalination* 392 (2016) 14–24.
- [22] Z. He, Y. Bai, H. Huang, J. Li, Huhetaoli, N. Kobayashi, Y. Osaka, L. Deng, Study on the performance of compact adsorption chiller with vapor valves, *Appl. Therm. Eng.* 126 (2017) 37–42.
- [23] A. Akisawa, M. Umair, K. Enoki, M. Nakayama, Static analysis of a new scheme of two stage refrigeration cycle with the combination of FAM-Z01 and FAM-Z05 adsorbents, *Int. J. Refrig* 92 (2018) 143–153.
- [24] S.-Y. Woo, H.-S. Lee, H. Ji, Y.-D. Kim, Adsorption isotherm model for analyzing the adsorption characteristics of water vapor to commercially available silica gel adsorbents for adsorption desalination applications, *J. Chem. Eng. Data* 66 (2021) 1144–1156.
- [25] C. Hackett, K.D. Hammond, Simulating the effect of the quadrupole moment on the adsorption of nitrogen in siliceous zeolites, *Microporous Mesoporous Mater.* 263 (2018) 231–235.
- [26] S.H. Madani, P. Kwong, F. Rodríguez-Reinoso, M.J. Biggs, P. Pendleton, Decoding gas-solid interaction effects on adsorption isotherm shape: I. Non-polar adsorptives, *Microporous Mesoporous Mater.* 264 (2018) 76–83.
- [27] P. Trens, R. Denoyel, J.C. Glez, Comparative adsorption of argon and nitrogen for the characterisation of hydrophobized surfaces, *Colloids Surf., A* 245 (1-3) (2004) 93–98.
- [28] M. Neitsch, W. Heschel, M. Suckow, Water vapor adsorption by activated carbon: a modification to the isotherm model of Do and Do, *Carbon* 39 (2001) 1437–1438.
- [29] M.A. Al-Ghouti, D.A. Da'ana, Guidelines for the use and interpretation of adsorption isotherm models: A review, *J. Hazard. Mater.* 393 (2020) 122383, <https://doi.org/10.1016/j.jhazmat.2020.122383>.
- [30] F. Raganati, M. Alfe, V. Gargiulo, R. Chirone, P. Ammendola, Isotherms and thermodynamics of CO₂ adsorption on a novel carbon-magnetite composite sorbent, *Chem. Eng. Res. Des.* 134 (2018) 540–552.
- [31] V.J. Inglezakis, S.G. Pouloupoulos, H. Kazemian, Insights into the S-shaped sorption isotherms and their dimensionless forms, *Microporous Mesoporous Mater.* 272 (2018) 166–176.
- [32] M. Thommes, K. Kaneko, A.V. Neimark, J.P. Olivier, F. Rodríguez-Reinoso, J. Rouquerol, K.S.W. Sing, Physisorption of gases, with special reference to the evaluation of surface area and pore size distribution (IUPAC Technical Report), *Pure Appl. Chem.* 87 (2015) 1051–1069.
- [33] K.S.W. Sing, Reporting physisorption data for gas/solid systems with special reference to the determination of surface area and porosity (Recommendations 1984), *Pure Appl. Chem.* 57 (1985) 603–619.
- [34] P.I. Ravikovitch, G.L. Haller, A.V. Neimark, Density functional theory model for calculating pore size distributions: pore structure of nanoporous catalysts, *Adv. Colloid Interface Sci.* 76-77 (1998) 203–226.
- [35] H.W.B. Teo, A. Chakraborty, Aluminium based zeolites and MOFs for adsorption cooling, *Trans. Jpn. Soc. Refrig. Air Condit. Eng.* 35 (2018) 377.
- [36] Y.-D. Kim, W.-S. Kim, Re-evaluation and modeling of a commercial diesel oxidation catalyst, *Ind. Eng. Chem. Res.* 48 (14) (2009) 6579–6590.
- [37] K. Thu, K.C. Ng, B.B. Saha, A. Chakraborty, S. Koyama, Operational strategy of adsorption desalination systems, *Int. J. Heat Mass Transf.* 52 (7-8) (2009) 1811–1816.
- [38] R.G. de Oliveira, D.J. Generoso, Influence of the operational conditions on the performance of a chemisorption chiller driven by hot water between 65°C and 80°C, *Appl. Energy* 162 (2016) 257–265.
- [39] K.C. Chan, C.Y. Tso, C. Wu, C.Y.H. Chao, Enhancing the performance of a zeolite 13X/CaCl₂–water adsorption cooling system by improving adsorber design and operation sequence, *Energy Build.* 158 (2018) 1368–1378.
- [40] C. Olkis, S. Brandani, G. Santori, Cycle and performance analysis of a small-scale adsorption heat transformer for desalination and cooling applications, *Chem. Eng. J.* 378 (2019), 122104.